Chem Soc Rev

REVIEW ARTICLE

View Article Online
View Journal | View Issue

Cite this: *Chem. Soc. Rev.*, 2025, **54**, 8434

Bioinspired micro-nano photonic materials

Chengben Liu,†[ab] Xiaoyu Hou,†[ace] Zixin Zhu†[ae] and Mingzhu Li *[ad]

The development of micro- and nano-scale photonic materials represents a cornerstone of modern science and technology. Nature, as a master architect, has served us with the most compelling and time-tested innovations and bio-designs. From the vibrant iridescent wings of butterflies to the anti-reflective eyes of moths, biological systems have long perfected the art of light manipulation through intricate micro- and nanoscale architectures. By decoding these biological mechanisms, harnessing nature-inspired design and interdisciplinary innovation, researchers unlock pathways to create materials with tailored optical properties, durability, and environmental adaptability. In the evolving landscape of photonic materials science, bioinspired micro-nano photonic materials emerge as a transformative frontier, bridging the ingenuity of biological evolution with cutting-edge photonic technologies. In this review, we provide an overview of research efforts on bioinspired micro-nano photonic materials, which offer multifunctional, adaptive, and sustainable solutions for next generation environmentally sustainable photonic materials and ultra-compact, energy-efficient photonic devices. We summarize the typical foundational principles of biological systems where nanostructures have evolved over millennia to master light. Furthermore, we highlight recent advances in bioinspired micro-nano photonic materials which have led to tremendous progress in eco-friendly structural color display, visual chroma sensor, high-security information encryption, energy-efficient functional optoelectrical devices, and so on. Finally, we discuss the challenges and prospects of bioinspired micro-nano photonic materials, including nature-inspired design, fabrication sustainability, and interdisciplinary synergy, for applications in telecom, energy, and biomedicine in the future.

Received 30th May 2025

DOI: 10.1039/d5cs00606f

rsc.li/chem-soc-rev

[a] *Laboratory of bio-inspired smart interface science, Technical Institute of Physics and Chemistry, Chinese Academy of Sciences, Beijing 100190, P. R. China. E-mail: mingzhu@mail.ipc.ac.cn*
[b] *School of Chemistry, Key Laboratory of Bio-inspired Smart Interfacial Science and Technology of Ministry of Education, Beihang University, Beijing 100190, P. R. China*
[c] *Key Laboratory of Green Printing, Institute of Chemistry, Chinese Academy of Sciences, Beijing 100190, P. R. China*
[d] *School of Future Technology, University of Chinese Academy of Sciences, Beijing 100049, P. R. China*
[e] *University of Chinese Academy of Sciences, Beijing 100049, P. R. China*
† Chengben Liu, Xiaoyu Hou and Zixin Zhu contributed equally to this work.

Chengben Liu

Chengben Liu received his bachelor's (2019) and Master's (2022) degree from China University of Petroleum (East China). He is now pursuing his PhD degree in the School of Chemistry, Beihang University. His current research focuses on the design, fabrication, and applications of bioinspired optoelectronic devices.

Xiaoyu Hou

Xiaoyu Hou received her bachelor's degree (2018) from Beijing Institute of Technology (BIT) and subsequently obtained her Master's degree (2021) and PhD (2025) from Institute of Chemistry, Chinese Academy of Sciences (ICCAS). Her research interest mainly focuses on the design and fabrication of bioinspired structural color materials.

1. Introduction

In the 21st century, micro-nano photonic materials promise to overcome the "bottleneck" of electronic interconnects, ushering in an era of photonic-driven computing with enhanced speed and sustainable optical materials with energy efficiency.[1] Here, micro-nano photonic materials refer to engineered systems featuring microscale or nanoscale structures that manipulate light *via* scattering, interference, diffraction, or resonance. Traditional photonic systems rely on bulk materials, often constrained by efficiency, scalability, and static functionality. As technology trends toward miniaturization, integrating photonic functionalities into microelectronic systems becomes critical.[2] The micro-nano photonic materials transcend the limitations of conventional optics by harnessing multiscale light manipulation.[3,4] These materials are not merely incremental advancements but foundational tools for a sustainable, interconnected future. The development of micro-nano photonic materials is propelled by urgent needs: sustaining digital growth, combating climate change, democratizing healthcare, and ensuring national security. Developing micro-nano photonic materials has emerged as a scientific and technological imperative.

Nature has served us with the most compelling and time-tested innovations and bio-designs.[5] Gaining wisdom from nature's genius forms the foundation of human survival and serves as the source of knowledge. Biological systems achieve extraordinary control of light–matter interactions through multiscale structural organization.[6–8] For instance, the iridescent wings of Morpho butterflies achieve vibrant structural color through a hierarchical architecture of alternating chitin–air layers.[9,10] The feathers of peacocks employ ordered melanin granules embedded in keratin matrices, leveraging coherent scattering to produce iridescence.[11] Beyond aesthetics, natural systems optimize energy utilization: chloroplasts in plant leaves organize thylakoid membranes into stacked grana to enhance light absorption and electron transport efficiency.[12–14] Corals employing porous, branching architectures redistribute weak light energy to their algal symbionts by lots of diffuse scattering.[15–17] Natural organisms employ a limited palette of biological materials such as chitin, keratin, and melanin to create hierarchical architectures with tailored optical functionalities.[6,18,19] The fascinating optical properties of biological systems are due to their exquisite micro-/nano structures refined through eons of evolution.[20–27]

By decoding these biological mechanisms, researchers unlock pathways to create materials with tailored optical properties, durability, and environmental adaptability. Bioinspired micro-nano photonic materials stand out as a transformative frontier, merging biological wisdom with advanced nanofabrication to create devices capable of precise light manipulation. Bioinspired designs enable on-chip photonics,[28–30] optical metamaterials,[31,32] and high-performance optoelectronics,[33] fostering advancements in eco-friendly colorful materials,[34,35] reflective display,[36,37] secure communication,[38–40] energy-efficient lighting,[41,42] efficient renewable energy[43–45] and so on. For instance, artificial structural color is more durable than pigments, astonishingly reducing reliance on dyes that fade or are toxic.[46,47] Anti-reflective coating mimicking the moth's eyes leads to efficient solar panels.[48] Passive radiative cooling coating inspired by the bio-white color offers a zero-energy solution for managing thermal radiation in buildings.[49,50] Photonic crystals (PhCs) following the opal lattice structure can control light propagation and emission, leading to applications in telecommunications, sensors, or solar cells (SCs).[51–53] With the rapid development of materials science and manufacturing processes, researchers combine nature's subtle bionic strategies with the ever-expanding library of advanced materials to create a new paradigm of function-oriented micro- and nano-photonic materials design. This cross-fertilization not only breaks through the boundaries of traditional material properties but also gives rise to innovative systems that combine bionic intelligence with engineering practicality. Therefore, it is important to summarize and review the development of this field. In this review, we will explore how humans learn from nature by following a three-step process: find and observe natural phenomena, analyze and extract physical mechanisms, and design and construct artificial bionic materials (Fig. 1). The review is divided into four sections. In the current chapter, we introduce the importance of bionics and bioinspired micro-/nano-photonic materials. Following this brief introduction, we summarize classic natural

Zixin Zhu

Zixin Zhu received her bachelor's degree from Beijing University of Chemical Technology. She is now pursuing a combined master's and doctoral degree at the University of Chinese Academy of Sciences (UCAS). Her research focuses on multifunctional micro-nano optical structure design and fabrication.

Mingzhu Li

Mingzhu Li is a full professor at Technical Institute of Physics and Chemistry, CAS, where her interests lie in the design, fabrication, and application of bioinspired micro-nano optical structures. She received her PhD degree from Institute of Chemistry, Chinese Academy of Sciences (ICCAS), and joined the Key Laboratory of Green Printing, ICCAS in 2008. In 2023, she moved to Technical Institute of Physics and Chemistry, CAS.

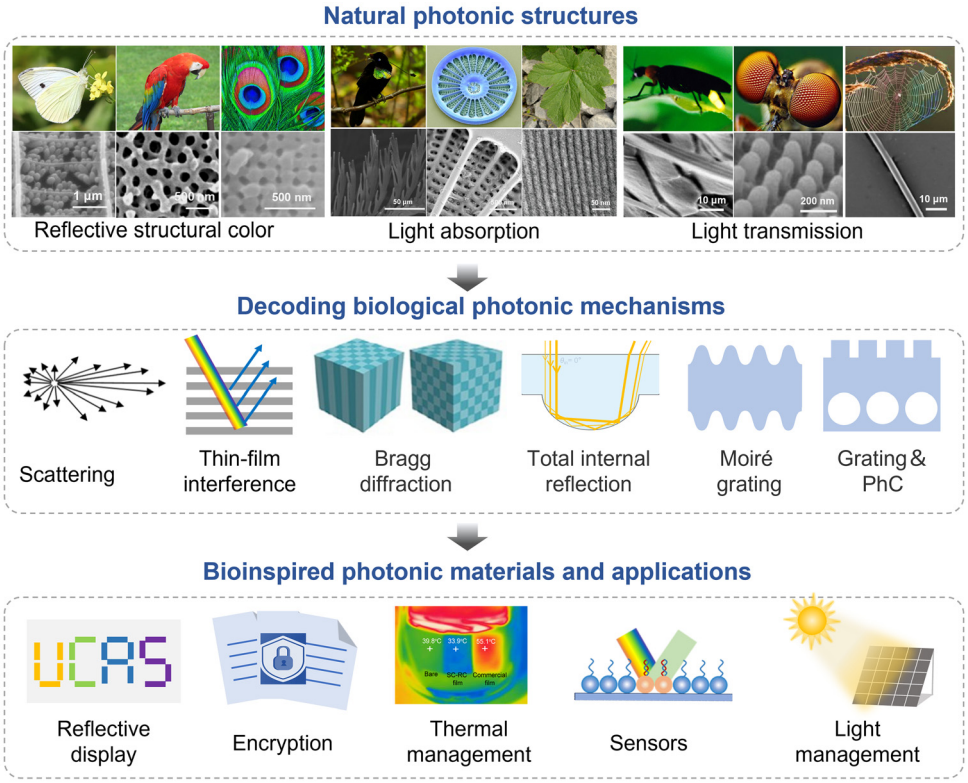

Fig. 1 Overview of the steps of biomimicry in micro-nano photonic materials, including investigating natural photonic issues, decoding underlying optical mechanisms, and bioinspired materials and applications. Part "reflective structural color" (from left to right) reproduced from ref. 20 with permission from Wiley-VCH, copyright 2016; ref. 21 with permission from National Academy of Sciences, USA, copyright 2012; and ref. 11 with permission from National Academy of Sciences, USA, copyright 2003. Part "light absorption" (from left to right) reproduced from ref. 22 with permission from Springer Nature, copyright 2018; ref. 23 with permission from Athena International Publishing B.V., copyright 2023; and ref. 24 with permission from Wiley-VCH, copyright 2010. Part "light transmission" (from left to right) reproduced from ref. 25 with permission from OSA, copyright 2013; ref. 26 with permission from Nature Publishing Group, copyright 2003; and ref. 27 with permission from OSA, copyright 2018.

inspirations and categorize them into three aspects briefly, including reflective structural color: from disordered to ordered, light absorption, and light transmission. In each part, we present some classic examples to render basic mechanisms underlying the unique optical properties found in nature and biology. By utilizing these natural mechanisms and versatile man-made materials, researchers have devoted significant efforts to creating many biomimetic materials with superior optical functions. We focus on the representative applications of reflective display, information security and encryption, optical sensors, and light and thermal management. In Section 3, we summarize the state-of-the-art advances in artificial optical materials and structures in those application fields. Finally, we provide an outlook on the future development of bioinspired micro- and nanophotonic materials, emphasizing their potential to drive innovation in diverse fields.

2. Natural inspirations and optical mechanisms

Bionic optics, a compelling field, is booming at an unprecedented rate. It is not just a simple imitation of nature, but also an in-depth exploration and creative application of the wisdom of nature. Biomimetics is the transfer of nature's superior design to technical applications.[54–57] How to do this? The logical and reasonable way is "Inverse design". Inverse design and fabrication of bioinspired micro-nano materials constitutes an interdisciplinary approach that leverages nature-inspired structural principles and advanced computational modeling to inversely engineer multiscale architectures with tailored functionalities, enabling breakthroughs in advanced materials, energy systems, and sustainable technologies. Then it is most significant to figure out the underlying optical mechanisms. The final step is to fabricate artificial materials.

This chapter focuses on the paradigm of bioinspired optical design, emphasizing two critical steps: identifying biological models exhibiting target functionalities and deciphering the underlying physical mechanisms. Only by rigorously understanding these mechanisms can researchers translate biological principles into functional artificial structures. For instance, the anti-reflective moth-eye motif has been replicated in silicon SCs, boosting efficiency *via* nanoimprinting. Crucially, mechanism-based design avoids blind mimicry. In exploring biological structures, scientists have found that the optical function of many organisms is not attributed to a single structure, but the result of multiple structures and mechanisms

working together and cooperating. This complex synergistic effect for the study of bionic optics has brought great challenges, but is also pregnant with unlimited opportunities. Thus, we try to abstract universal principles that transcend specific biological contexts in the next content. According to the interaction between light and micro-nano structures, we categorize some classical bioinspiration into three groups, namely light reflection, light absorption, and light transmission.

2.1 Reflective structural color: from disordered to ordered

Coloration represents a milestone of evolutionary adaptation, driving critical survival strategies across life. In nature, colors are intricately linked to ecological survival, enabling camouflage against predators, sexual signaling for mate selection, aposematism to deter threats, and thermoregulation through light reflection. These functions are achieved through three principal mechanisms: pigment-based coloration, bioluminescence, and structural coloration. While pigments and bioluminescence have evolved to address specific needs, structural colors—a product of nanoscale architecture—stand out as a paradigm of evolutionary optimization, offering unparalleled durability and optical versatility.

Structural coloration arises from the interaction of light with subwavelength-scale architectures. These nanostructures manipulate light *via* fundamental optical phenomena, including interference, diffraction, and coherent scattering.[58] The evolutionary advantage of structural colors lies in their inherent robustness and energy efficiency. Unlike pigments, which degrade under UV exposure or oxidative stress, structural colors remain vibrant as long as their nano-architectures remain intact—a feature critical for long-term signaling in harsh environments. Furthermore, structural systems can be easily tunable. Organisms such as cephalopods and chameleons have evolved dynamic structural colors by reconfiguring the spacing of reflective platelets or chromatophores, enabling real-time camouflage or communication. This tunability is governed by precise control of structural parameters, including lattice periodicity, layer thickness, and refractive index contrast, which collectively determine the spectral and angular response of reflected light.

2.1.1 Disordered systems. To systematically elucidate the optical principles underlying structural colors, we categorize them based on their degree of order, spanning disordered to highly organized architectures. When a material is disordered, that is, its refractive index distribution is inhomogeneous, at which point incoherent scattering is the dominant phenomenon (Fig. 2a). In such systems, light is scattered evenly in all directions, resulting in the appearance of white color. The striking white coloration serves critical ecological functions, including thermoregulation, camouflage, and intraspecific signaling. For instance, the wings of the *Pieris rapae* butterfly exhibit a striking white coloration.[20] This whiteness arises from sophisticated nanostructures within the wing scales. The scanning electron microscopy (SEM) image reveals the inside structure of the scales featuring a disordered array of pterin-based ellipsoidal pigment particles embedded within a keratin scaffold. It's discovered that these composite structures exhibit a

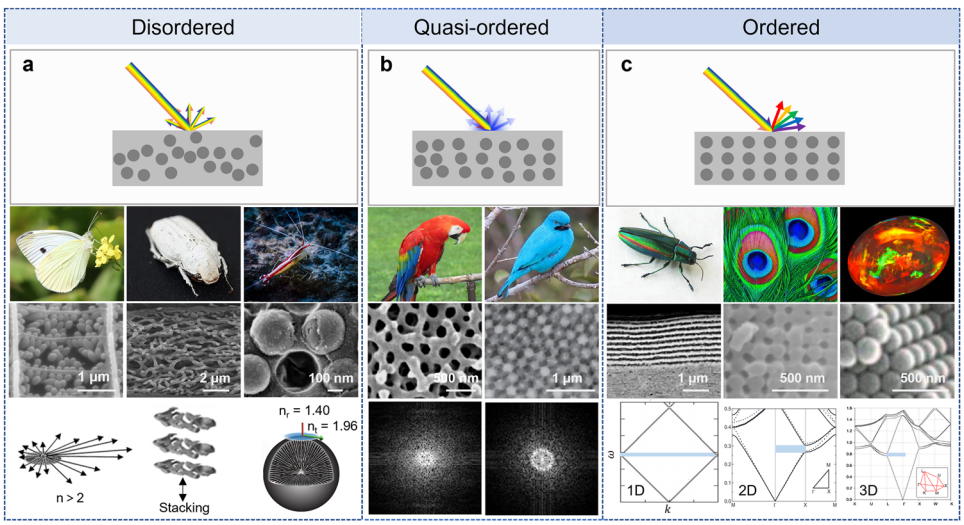

Fig. 2 The physical mechanisms and natural examples for structural coloration from disordered to ordered. (a) Disordered structures achieve wavelength-independent all-directional reflection, resulting in a white color. *Pieris rapae* (left), *Cyphochilus* beetle (center), and Pacific cleaner shrimp (*Lysmata amboinensis*, right), the corresponding SEM images of their disordered structures, and the extracted optical structure models. Reproduced from ref. 20 with permission from Wiley-VCH, copyright 2016; ref. 61 with permission from Wiley-VCH GmbH, copyright 2015; ref. 62 with permission from Springer Nature, copyright 2023. (b) Quasi-ordered structures exhibit weak angle-independent coloration from coherent scattering. The feathers of the Scarlet macaw (*Ara macao*, left) and *Cotinga maynana* (right) all exhibit non-iridescent blue color, and the corresponding SEM images and 2D Fourier transform spectra are given. Reproduced from ref. 21 with permission from National Academy of Sciences, USA, copyright 2012; ref. 66 with permission from Royal Society of Chemistry, copyright 2009. (c) Ordered structures, that is, PhC, enable iridescent color leveraging constructive and destructive interference. 1D PhC structure of jewel beetle (*Chrysochroa fulgidissima*, left), 2D PhC structure of peacock (*Pavo muticus*, center),3D PhC structure of natural opals (right). SEM images and photonic band structures are provided. Reproduced from ref. 74 with permission from John Wiley & Sons, Ltd, copyright 2020; ref. 11 with permission from National Academy of Sciences, USA, copyright 2003.

high effective refractive index of 1.75–1.9. Especially, pigment particles can achieve a refractive index exceeding 2.0, which is rare in nature. In addition, the pterin pigments exhibit strong ultraviolet absorption (<400 nm), which concomitantly elevates the real refractive index at shorter visible wavelengths. According to the Mie modeling, a high refractive index enhances scattering intensity considerably. Further, the anisotropic geometry of the particles is optimized. Computational modeling confirms that ellipsoidal morphologies, compared to spherical counterparts of equivalent volume, significantly enhance scattering cross-sections. Consequently, a sophisticated integration of scattering enhancement and spectral absorption underlies the whiteness mechanism.

Sometimes brilliant structure designs help broaden the selection of materials, meaning achieving whiteness will not be limited to high refractive index. Normally, when the refractive index is lower, increasing material thickness must be done to achieve whiteness. However, in nature, another ingenious structure for well-optimized whiteness was uncovered in the scales of the beetle genus *Cyphochilus*.[59,60] The *Cyphochilus* beetle broke the rule since it possesses a fabulous white color with thin scales *ca.* 7 μm in thickness. Meanwhile, their scales are composed of chitin with a refractive index of around 1.55–1.56 and have a disordered network of fibers orienting vertically to the direction of the incident light. Lorenzo *et al.* proved that anisotropic light transport in such a structure boosts scattering strength, facilitating the achievement of a high white reflectance (>0.8) across the visible wavelength range.[61] Achieving intense whiteness in aqueous environments presents unique challenges for the relative refractive index of $n_{rel} = n_{material}/n_{water}$ is lower than that in air ($n_{rel} = n_{material}/n_{air}$). Nature provides novel problem-solving strategies inspired by biological systems. The Pacific cleaner shrimp (*L. amboinensis*) reveals the important role of birefringence in obtaining whiteness.[62] Cryo-electron microscopy unveiled densely packed nanospheres within submicron-thick chromatophores of the shrimp's white markings. These particles consist of radially aligned isoxanthopterin molecules, creating optical anisotropy with distinct refractive indices ($n_{radial} = 1.4$ *vs.* $n_{tangential} = 1.96$). Numerical simulation demonstrates that a polydispersity of 10% could suppress structural color while maintaining broadband reflectance. Crucially, the particles' anisotropic refractive index distribution reduces near-field interactions and spatial crowding effects that plague conventional isotropic scatterers. This dual strategy enables higher visible-light reflectance compared to isotropic counterparts across diverse packing densities. Such bioinspired structural principles are revolutionizing radiative cooling technologies. By decoupling optical performance from intrinsic material properties, these whiteness models exemplify nature's strategy to overcome physical limitations through topology optimization. This paradigm shift informs next-generation photonic materials for sustainable cooling, energy-efficient architecture, and low-carbon manufacturing, underscoring the transformative potential of bioinspired disorder engineering in addressing global thermal management challenges.

2.1.2 Quasi-ordered systems. The transition from disordered to ordered photonic architectures in biological systems reveals a remarkable sensitivity of optical phenomena to nanoscale organization. By increasing the degree of order slightly, it is interesting to see drastic changes in optical phenomena, ranging from whiteness to coloration with no angular dependence even to weak iridescence (Fig. 2b). Unlike purely disordered systems dominated by incoherent scattering, quasi-ordered nanostructures exhibit partial spatial correlations that introduce weak coherence to scattered light.[63–65] This semi-ordered regime balances evolutionary trade-offs: it avoids the angular sensitivity of perfect PhCs while achieving more tuned colors than fully random systems. Such angle-independent coloration provides critical adaptive advantages, allowing organisms like birds to maintain consistent visual signals across diverse lighting conditions—essential for mate recognition, territorial displays, or predator evasion. In avian systems, quasi-order is typically mediated by β-keratin, a versatile structural protein that self-assembles into two distinct photonic motifs. One is a channel-type nanostructure widely found in the eastern bluebird *S. sialis* with β-keratin bars and air channels in tortuous and twisting forms.[66] Similarly, the non-iridescent blue feather barbs of the scarlet macaw stem from amorphous diamond-structured keratin rods unraveled by Yin *et al.*[21] The other one is a sphere-type nanostructure constructed by nearly close-packed spherical air cavities found in the *Cotinga maynana*.[66]

Recent synthetic advances have successfully replicated quasi-ordered photonic architectures. For example, photonic glasses based on colloidal particles or bottlebrush block copolymers can mimic the short-range order found in nature while offering tunable optical responses.[67,68] These artificial analogues benefit from scalable fabrication techniques, such as colloidal self-assembly and thermal annealing, and can produce non-iridescent structural color across a broad spectrum. Moreover, the development of optical modeling approaches—such as Monte Carlo simulations that incorporate both multiple scattering and absorption effects—has enabled predictive control over color properties in disordered media.[69,70] These developments establish a unified framework for engineering angle-independent structural colors across both biological and synthetic systems.

Quantifying the relationship between structural order and optical output remains challenging due to the nuanced interplay of spatial correlations. Fourier analysis has emerged as a critical tool, decomposing electron microscopy images into reciprocal space representations.[71] The resulting power spectra reveal characteristic ring patterns—sharp rings indicate high periodicity, while diffuse halos signify disorder. Intermediate states exhibit both features, confirming the coexistence of short-range order and long-range disorder in quasi-ordered systems. The structure factor $S(q)$ serves as a fundamental metric for characterizing the degree of spatial order in these systems. It quantifies how incident waves are scattered by the material's internal structure, with its spectral features directly reflecting the system's correlation properties.[72,73] These structural

correlations enable weak but significant interference effects, as quantified by the structure factor, which modulates the phase relationships between scattered waves. In quasi-ordered structures, $S(q)$ plays a central role in determining the resulting structural colors by governing both the intensity of coherent scattering and the wavelength selectivity of reflected light. Although these structures lack perfect periodicity, they typically exhibit statistically preferred length scales, which manifest as broadened peaks in the structure factor. The position of these peaks determines the dominant reflected wavelength—and thus the hue of the structural color—while their sharpness influences the spectral purity: sharper peaks indicate stronger wavelength selectivity and result in more saturated colors. Therefore, $S(q)$ not only reveals the degree of spatial order but also directly dictates the spectral characteristics of the optical response. Despite lacking perfect crystalline order, quasi-ordered architectures achieve functional optical performance through evolutionary optimization. Their design principles—balancing manufacturability with optical efficiency—inspire biomimetic materials for applications requiring angle-independent colors, such as anti-glare coatings and durable textile dyes. By decoding how biological systems navigate the order–disorder continuum, researchers gain insights into nature's strategies for engineering light at subwavelength scales.

2.1.3 Ordered PhCs. When materials are arranged periodically at length scales commensurate with visible light wavelengths, their interaction with light is governed by interference phenomena. Constructive and destructive interference of reflected or transmitted waves generates vivid, angle-dependent structural colors—a phenomenon termed iridescence. Among ordered photonic systems, PhCs represent the most archetypal class, defined by their periodic modulation of refractive index in one, two, or three spatial dimensions (Fig. 2c). These crystals exhibit photonic bandgaps, frequency ranges where light propagation is prohibited, enabling precise spectral control through structural design. Below, we elucidate the physical mechanisms of one dimensional (1D), two dimensional (2D), and three dimensional (3D) PhC and their biological manifestations.

1D PhC consists of alternating planar layers of high- and low-refractive-index materials. Light waves reflecting at each interface interfere coherently, with the phase difference determined by layer thickness and refractive indices. According to Bragg's law, constructive interference occurs when:

$$2n_{\text{eff}}d\sin\theta = m\lambda$$

where λ is the wavelength, n_{eff} is the refractive index, d is the spacing, m is the diffraction order, and θ is the angle of incidence. This mechanism produces iridescent colors in systems such as jewel beetles, where 12 to 16 thick and thin layers alternating reflect green or red light,[74] and Morpho butterfly wings, where chitin–air multilayers selectively reflect blue wavelengths. 1D systems excel in narrowband spectral filtering, ideal for optical coatings and angle-tunable sensors.

2D PhC features periodic structures in two dimensions, such as hexagonal arrays of cylindrical rods or holes. Light propagates in-plane, with photonic bandgaps emerging from periodic variations in the transverse direction. For example, the iridescent eye spots on peacock (*Pavo cristatus*) feathers derive their brilliance from 2D PhC lattices within barbules.[11] Each barbule contains melanin rods embedded in a keratin matrix, arranged in a square lattice with a periodicity of ~140 nm. This lattice selectively reinforces green and blue wavelengths (450–500 nm) *via* Bragg scattering while suppressing others, creating angle-dependent metallic hues: incident light undergoes interference at melanin–keratin interfaces, with only wavelengths satisfying the Bragg condition being strongly reflected, while others are suppressed by destructive interference, resulting in angle-dependent iridescence.

3D PhC exhibits periodicity in all spatial dimensions, akin to atomic lattices in crystals. Natural opals exemplify this class, comprising close-packed silica spheres in a face-centered cubic (FCC) arrangement. Incident light undergoes Bragg diffraction across multiple crystallographic planes, generating iridescent "play-of-color" that shifts with viewing angle. The photonic bandgap in 3D situations can be calculated by the following formula:

$$2d\sqrt{n_{\text{eff}} - \sin^2\theta} = m\lambda$$

where λ is the wavelength, n_{eff} is the refractive index, d is the spacing, m is the diffraction order, and θ is the angle of incidence. 3D systems offer omnidirectional bandgaps and enhanced light confinement, making them candidates for low-threshold lasers and full-color displays. Their structural complexity, however, poses fabrication challenges.

2.1.4 Polarization manipulation in biological systems. Furthermore, the optical ingenuity of biological systems extends far beyond color generation, encompassing sophisticated control over light polarization.[75] Many animals can detect polarized light, which is highly related to navigation and orientation. These functionalities often arise from cholesteric liquid crystal-like arrangements, where hierarchical helicoidal structures selectively reflect one type of circularly polarized light but do not respond to the other circularly polarized light.[76] Helicoidal architectures are widespread, observed across diverse taxa such as beetles and butterflies.[77,78] Among them, one of the most famous organisms is *Chrysina gloriosa*, which has an iridescent metallic green outlook and can selectively reflect left circularly polarized light (Fig. 3a).[79] Its iridescent green appearance originates from a multilayered cuticle with helicoidally stacked chitin fibrils, each layer rotated by a fixed angular increment. This configuration creates a periodic refractive index modulation along the helical axis, satisfying the Bragg condition for left-circularly polarized (LCP) reflection:

$$\lambda = 2np$$

where n is the average refractive index, and p denotes the helical pitch—the axial distance required for a 180° fibril rotation. When illuminated with unpolarized light, only LCP components matching the pitch-proportional wavelength ($\approx$530 nm for green) undergo constructive interference, while right-circularly polarized (RCP) light is transmitted. Experimental validation using quarter-wave plates and polarizers

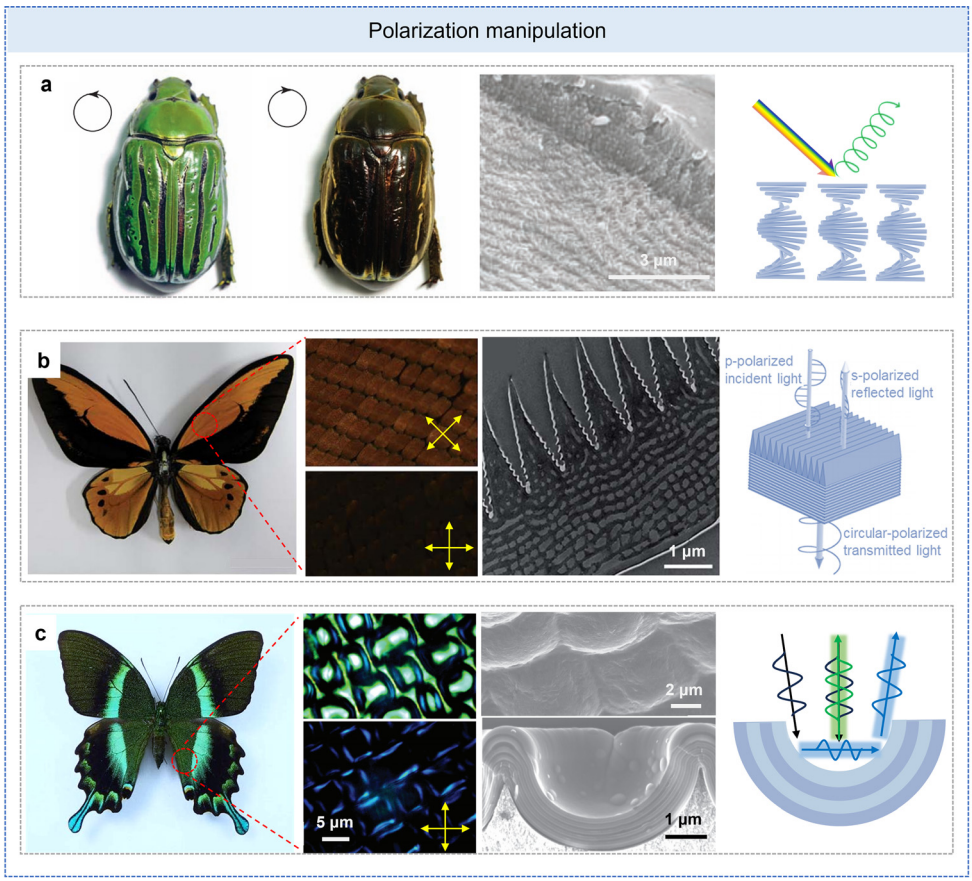

Fig. 3 Biological examples of manipulating light's polarization state and corresponding schematic diagram of the optical principle. (a) Photographs of the beetle *Cataglyphis gloriosa* under left and right circular polarizers. SEM image showing chiral helical nanostructure. Reproduced from ref. 79 with permission from American Association for the Advancement of Science, copyright 2009. (b) Photograph of *Ornithoptera croesus lydius* and optical images of scales at 45° and 0/90° azimuth under crossed polarizers. TEM image exhibiting a composite structure comprising a grating and a multilayer. Reproduced from ref. 80 with permission from Royal Society of Chemistry, copyright 2014. (c) The green color of the *Papilio blumei* butterfly results from color blending. Optical micrographs observed without (left) and with (right) cross-polarizers. SEM (top) showing the concavities of scales and SEM (bottom) of a biomimetic sample showing a conformal multilayer stack. Reproduced from ref. 81 with permission from Nature Publishing Group, copyright 2010.

confirms this mechanism: blocking LCP components eliminates the green reflectance. The ubiquity of these architectures has a universal principle: subwavelength periodicity in dielectric anisotropy enables polarization manipulation. By emulating these designs, researchers have engineered biomimetic metasurfaces for optical encryption and polarization-sensitive imaging, demonstrating nature's enduring role in advanced photonic technologies.

Another mechanism for achieving polarization-sensitive color was demonstrated by Zhang and coworkers through a sophisticated dual-architecture design within the orange scales in the butterfly *Ornithoptera croesus lydius*.[80] As illustrated in Fig. 3b, the scale integrates two photonic components: surface-level tapered triangular gratings and subsurface multilayer reflectors (alternating chitin/air layers). This hierarchical configuration generates coloration through synergistic light–matter interactions: the upper grating produces zero-order diffraction while the underlying multilayer induces first-order interference, collectively enhancing orange wavelength reflectance. Polarization sensitivity emerges from azimuth-dependent optical transformations. Under crossed polarizer–analyzer configurations, reflected light intensity exhibits angular modulation, reaching minimum intensity when scale ridges align parallel/perpendicular to the incident polarization axis, yet recovering maximum reflectance at ±45° orientations. Through simulations, the team elucidated the polarization conversion mechanism. The tapered grating geometry functions as a quarter-wave plate, inducing phase retardation that converts p-polarized incident light into s-polarized output when illuminated at 45° incidence.

The optical complexity of biological systems often arises from the integration of hierarchical structures, enabling multifunctional performance beyond singular mechanisms. A striking example is the Southeast Asian butterfly *Papilio palinurus*, which achieves simultaneous polarization conversion and color blending through a meticulously organized multiscale photonic architecture (Fig. 3c).[81] In this case, the wing scales feature concave microstructures (5–10 μm diameter) arranged in ordered arrays, each comprising a dual-level design. A multilayer stack of

alternating chitin and air films generates yellow reflectance *via* Bragg interference at near-normal incidence. The curved sidewalls of each concavity impose oblique illumination angles on the underlying multilayers, inducing a blue shift through angularly tuned constructive interference. This geometric tuning creates spatially separated color domains—yellow from cavity bases and blue from sidewalls—which blend perceptually into a vibrant green. Moreover, the concave geometry also introduces polarization conversion. Light incident on cavity edges undergoes double reflection, imparting a geometric phase shift that converts linearly polarized incident light to cross-polarized states. This polarization conversion is experimentally validated by placing wing scales between crossed polarizers: only retroreflected edge segments retain detectable intensity, while normally reflected central light is extinguished. Such dual functionality—spectral blending and polarization modulation—stems from the hierarchical coupling of micro- and nanoscale features. This integrative strategy inspires novel optical devices, such as polarization-encoded security tags.

In summary, structural colors epitomize nature's mastery of optics, merging evolutionary fitness with nanoscale engineering. By decoding their underlying principles—from photon bandgap engineering to multilayer interference—researchers can harness them to advance photonic materials, ecological monitoring tools, and sustainable industrial applications.

2.2 Light absorption

The efficient capture of solar energy has emerged as a critical scientific frontier, driven by escalating global energy demands and the urgent need to transition from fossil fuels to renewable resources. As the largest accessible renewable energy flux, solar radiation offers a sustainable pathway to meet these challenges, as long as we overcome limitations in photon management, energy conversion, and storage. Traditional photovoltaic and photocatalytic technologies often struggle with inefficiencies stemming from spectral mismatch, reflection losses, and charge recombination. Herein lies the promise of biomimicry: over billions of years, evolutionary pressures have refined biological systems to optimize light harvesting under extreme environmental constraints, from sun-baked deserts to aphotic ocean depths. These organisms achieve remarkable efficiencies through nanoscale architectures that defy conventional engineering paradigms, offering scientists enormous brilliant ideas to design incredible materials.[82]

Biological light-harvesting architectures span a wide range of length scales—from nanometers to microns—each exploiting distinct physical principles to optimize solar energy capture. At the nanoscale, structures interact with light primarily *via* near-field effects, enabling sub-diffraction light confinement and enhanced absorption. In the subwavelength regime, periodic or quasi-periodic features produce interference-based phenomena including diffraction, Bragg scattering, and photonic bandgap effects. At the micron scale, geometric optics governs light behavior—*via* refraction, lensing, and multiple scattering—allowing for extended photon path lengths within absorbing tissues. Notably, many biological systems combine multiple hierarchical features to achieve broadband absorption, where micron-scale light focusing enhances delivery to subwavelength structures, which in turn channel photons toward nanoscale absorbers. This integrated multiscale strategy not only improves light-trapping efficiency across the visible spectrum (400–700 nm) but also offers critical design insights for bioinspired optical materials.

Biological systems have evolved sophisticated strategies to maximize photon capture, primarily through two complementary approaches: boosting multiple scattering and enhancing light concentration *via* structural engineering. Among natural light-absorbing materials, ultra-black surfaces with little reflectance are observed across diverse taxa, including araneids, avians, and lepidopterans.[83] These organisms provide critical insights for developing robust, lightweight absorbers with multifunctional capabilities. Zhang *et al.* revealed that the synergistic effect of inverse-V ridges and subwavelength nanoholes was responsible for ultra-black coloration. Experimental and computational analyses of *Troides aeacus* black scales demonstrated that inverse-V ridges enhance light penetration depth, directing photons into subsurface nanohole layers where near-total absorption occurs.[84] Recently, Alexander and colleagues systematically studied the nanostructure and physical mechanisms of ultra-black wings in butterflies (Fig. 4a).[85] It has been proven that expanded trabeculae and steep ridges in the scales can decrease reflectance by 16-fold and increase multiple scattering. These biological principles mirror those governing synthetic ultra-black materials, emphasizing two cardinal rules: maximization of photon trapping through multiscale roughness, and enhancement of effective absorption cross-sections *via* hierarchical porosity. Different from butterflies, the super black bird of paradise feathers provide another structural absorption mechanism with highly modified microstructures (Fig. 4b).[22] McCoy *et al.* observed vertically tilted barbule arrays creating deep, curved cavities leading to more light absorption *via* multiple scattering. Ultrablack-inspired architectures now guide innovations in aerospace coatings that reduce radar cross-sections, optical sensors that improve signal-to-noise ratios, and space technologies that minimize stray light in telescopes.

Beyond animal photonic systems, terrestrial plants have evolved hierarchical architectures optimized for solar energy harvesting through 3.8 billion years of photosynthetic evolution. Natural leaves achieve quantum efficiencies exceeding 90% in the light-harvesting process, a feat enabled by chloroplast nanostructures (Fig. 4c).[24,86,87] The 3D arranged lamellar membrane systems within chloroplasts demonstrate remarkable photon management strategies through their extended interfacial architectures. These biomolecular assemblies achieve enhanced photon capture efficiency through synergistic mechanisms: simultaneous light absorption at pigment–protein complexes, recurrent internal reflection across adjacent membranes, and diffusive scattering within confined luminal spaces. Such nanoscale light confinement extends optical path lengths compared to planar configurations. Inspired by this hierarchical structure, many high-performance photocatalysts have been developed, aiming to efficiently utilize solar energy.[88,89]

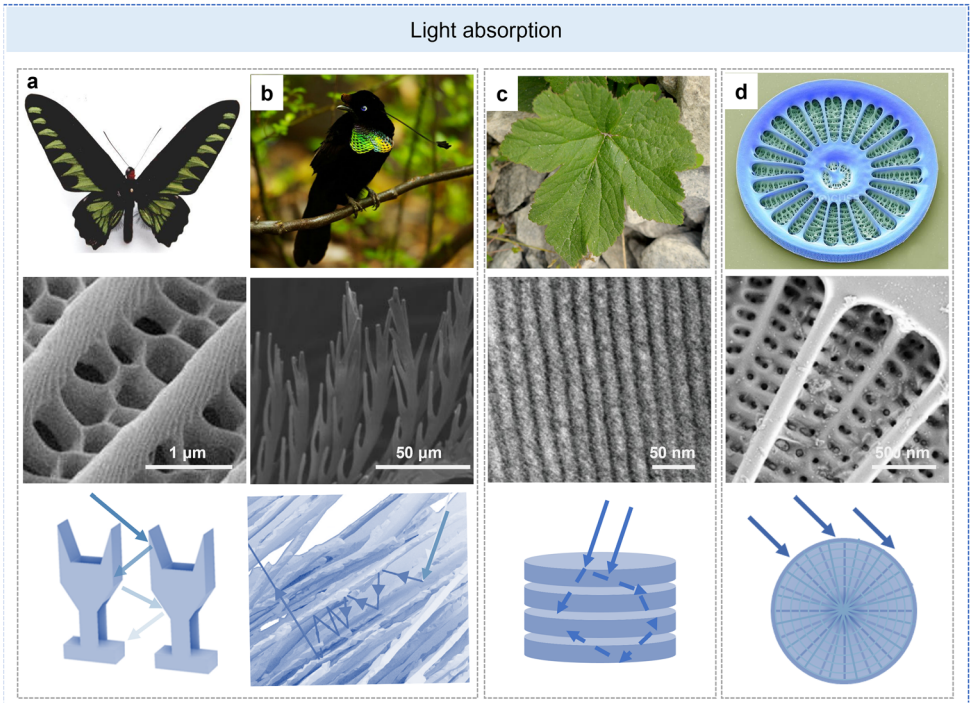

Fig. 4 Classic biological instances with light absorption function, the corresponding SEM images of their structures, and the strategy of designing intricate structures for highly efficient light absorption. (a) *Trogonoptera brookiana*. Reproduced from ref. 85 with permission from Springer Nature, copyright 2020. (b) Wahnes' Parotia *Parotia wahnesi*. Reproduced from ref. 22 with permission from Springer Nature, copyright 2018. (c) Green leaves. Reproduced from ref. 24 with permission from Wiley-VCH, copyright 2010. (d) *Arachnoidiscus ehrenbergii*. Reproduced from ref. 23 with permission from Athena International Publishing B.V., copyright 2023.

In terms of light concentration, among the organisms that developed complex photonic architectures, particular interest has recently been focused on diatoms.[42,90] Diatoms, unicellular microalgae responsible for 20–25% of global photosynthetic oxygen production, thrive in aquatic environments through exquisitely engineered silica exoskeletons (frustules). The diatom's silica frustule (cell wall) contains periodic or quasi-periodic distributions of nanopores ranging from some tens of nanometers to one micron.[91,92] These nanoporous architectures, particularly in species like *Arachnoidiscus ehrenbergii*, can selectively reflect/scatter specific photons to enhance light harvesting efficiency (Fig. 4d).[23] SEM reveals heterovalvar frustules comprising two morphologically distinct valves: a planar central region surrounded by radially aligned slits and concentric rings of progressively shrinking pores. The valve's internal costa system radiates from a central flange, creating wavelength-dependent optical phenomena. Under visible light illumination, interference between diffracted waves from individual pores generates coherent hotspots at the frustule center. In contrast, UV wavelengths experience minimal concentration due to destructive phase matching, inherently shielding photosynthetic machinery from harmful radiation. This spectral selectivity combining visible light focusing with UV rejection shows evolutionary optimization for both energy capture and photoprotection. Parallel to diatoms, Ruben *et al.* found terrestrial plants like Rosa 'El Toro' employ epidermal micro-nanostructures to synergize anti-reflection and light concentration.[93] It's because the micropapillae act as microlenses, focusing incident light into the petal's interior, which indirectly prolongs the average optical path length and finally boosts light absorption.

2.3 Light transmission

Improving light transmission efficiency—the enhanced ability to propagate photons with minimal energy loss—is a cornerstone of optical technologies, governing performance in applications ranging from illumination, display, telecommunications, and energy systems. High transmission efficiency ensures energy conservation, signal fidelity, and spatial resolution, particularly in low-light environments or miniaturized devices. In nature, organisms have evolved intricate photonic architectures to optimize light transmission, balancing energy expenditure with functional demands. These biological solutions often surpass synthetic counterparts in efficiency and multifunctionality. Below, we explore three paradigms of natural light transmission optimization and their physical mechanisms.

Bioluminescence is a large part of light transmission and refers to the phenomenon in which an organism converts chemical energy into light energy through chemical reactions. This phenomenon is widespread among marine organisms, plants, and insects, playing diverse critical roles for both the organisms themselves and their ecological surroundings—including communication and information exchange, predation and defense mechanisms, as well as physiological regulation and energy metabolism. However, reflections at the interface

prevent the organism from emitting light internally, reducing the organism's adaptability to the environment and the probability of survival. Through natural evolution and selection, many organisms have specialized structures that aid in light extraction and enable them to survive in harsh competition. There are many great instances. Here, fireflies are our main characters (Fig. 5a).[25] Fireflies achieve remarkable bioluminescence efficiency through hierarchical nanostructures on their lantern cuticles. The lantern surface is textured with asymmetric, tilted microribs that function as a diffraction grating. These microstructures reduce total internal reflection (TIR) at the cuticle-air interface by redirecting trapped photons outward, minimizing backscattering. This design enables fireflies to broadcast mating signals over long distances with minimal metabolic cost, as photons generated by luciferase reactions are channeled directionally rather than isotropically. Inspired by firefly lanterns, researchers have engineered biomimetic light-emitting diodes (LEDs) with nanostructured encapsulation layers.[94,95] Such designs are pivotal for energy-efficient displays, surgical lighting, and wearable optoelectronics.[42]

Besides, decreasing light reflection from the interface is an ingenious way to increase transmission efficiency. Meanwhile, it is especially conducive for visual imaging and escaping from enemies. Several mechanisms have been observed to achieve anti-reflective structures in the eyes and wings of insects (Fig. 5b). For instance, transparent wings of *Cephonodes hylas* (bee hawkmoth) utilize nanopillar arrays to minimize surface reflections, enabling near-invisible camouflage during flight.[96] The main mechanism is that nanopillar arrays gradually change the average refractive index, smoothing the impedance mismatch of the interface. Moths employ similar subwavelength nanostructures to maximize light transmission in dim environments. Their compound eyes feature hexagonal arrays of conical nipples that create a graded refractive index transition from air to the corneal chitin. This gradient suppresses Fresnel reflections across broad angles and wavelengths, achieving extreme transmittance. For moths, enhanced light transmission improves nocturnal vision sensitivity, while hawkmoth wings reduce predator detection by eliminating glare.[26] Nowadays, bioinspired anti-reflective structures are revolutionizing photovoltaics and optical sensors. These coatings also benefit camera lenses, laser optics, and augmented reality displays by eliminating ghost imaging.

From a different aspect of thinking, a highly efficient transmission means that light can propagate longer. In nature, fiber-optic systems achieve low-loss light transmission through cylindrical waveguiding (Fig. 5c). Remarkably, studies have provided many interesting results about using natural spider silk as an optical fiber.[27,97,98] Similarly, the heart cockle (*Corculum cardissa*) embeds lucent calcium carbonate fibers within its shell, channeling sunlight to photosynthetic symbionts, sustaining photosynthesis in sediment-buried habitats.[99] Cockle fibers enable mutualistic energy harvesting.

Nature's mastery of light transmission stresses the synergy between evolutionary adaptation and physical law. By decoding biological designs from firefly gratings to spider waveguides, researchers are transcending traditional optical engineering, achieving unprecedented efficiency in illumination, imaging, and energy harvesting.

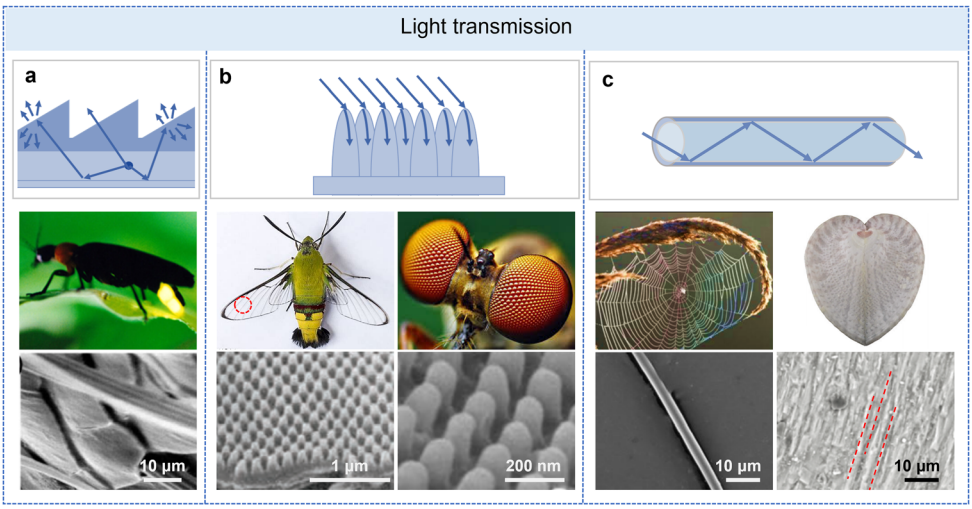

Fig. 5 Examples of light transmission structures in the natural world. (a) Schematic illustration demonstrating reduced total internal reflection and increased emission. The abdominal segments of *Photuris* fireflies with complex optical structures can improve light extraction. SEM images of misfit scales. Reproduced from ref. 25 with permission from OSA, copyright 2013. (b) Diagrams of the gradient index mechanism for antireflection (enhancing transmission) of the wings of bee hawkmoth and moth eye. Photographs of *Cephonodes hylas* (bee hawkmoth) and moth, and the corresponding SEM characterization of nanostructure. Reproduced from ref. 96 with permission from Zoological Society of Japan, copyright 1997; ref. 26 with permission from Nature Publishing Group, copyright 2003. (c) Schematic diagram of light transmission fiber structure. Spider silk' photograph and SEM image are given. Reproduced from ref. 27 with permission from OSA, copyright 2018. Heart cockle (*Corculum cardissa*) cross-sectional SEM of shell window showing fibrous prisms acting like fiber bundles (red line refers to fiber orientation). Reproduced from ref. 99 with permission from Springer Nature, copyright 2024.

3. Applications of bioinspired optical materials

3.1 Reflectivity display

Micro/nano photonic structures play a significant role in the field of display technology for their ability to generate structural colors and dynamically modulate light.[100,101] Inspired by natural photonic systems such as the Morpho butterfly wings, artificial structural color pixels based on PhCs and plasmonic nanostructures can achieve brilliant color display without relying on traditional pigments.[102–104] These structures exploit geometry-dependent optical effects—such as the photonic bandgap in PhCs and localized surface plasmon resonance in metallic nanostructures—to selectively filter or reflect specific wavelengths, thereby producing various structural colors. This color generation mechanism not only eliminates the need for high-power backlighting but also ensures stable and vibrant color reproduction under bright ambient lighting conditions, making it an ideal solution for energy-efficient applications including electronic paper, smart labels, and outdoor signage. Furthermore, their superior performance characteristics including wide color gamut, high visibility under daylight conditions, and environmentally friendly position them as promising candidates for next-generation display technologies.[105,106] Beyond static color, some biological organisms, such as chameleons[107–109] and cuttlefish,[110] achieve dynamic color changes through real-time modulation of nanostructures in their skin. Inspired by this, researchers have developed light-, thermal-, and ion-responsive materials by integrating stimuli-responsive photonic structures, enabling full-color tuning, thermal sensing, and synchronized electro-optical output. These biomimetic systems bridge the gap between static and adaptive photonic displays, opening new opportunities for intelligent visual technologies.

3.1.1 Imaging. Structural color pixels, formed from PhC structures, are widely used in reflectivity display technology due to their ability to manipulate light *via* periodic nanostructures, especially 3D PhC based on opal and inverse opal structures.[111,112] These PhC structures are typically fabricated through scalable self-assembly methods. Furthermore, incorporating materials with varied functionalities into these structures enables the realization of diverse functional properties. For example, Li *et al.* fabricated biocompatible PhC patterns with microscale precision based on silk fibroin inverse opals (SIOs) (Fig. 6a–d), employing two distinct approaches: (1) patterning polystyrene colloidal crystal templates *via* ethyl acetate dissolution and subsequent silk infiltration, and (2) direct modulation of SIO lattice constants *via* methanol/water solvent deposition.[113] By utilizing the properties of silk fibroin's structural polymorphism, such photonic lattices can undergo multi-spectral responses through molecular chain rearrangement, allowing for the generation of colorful patterns. Besides, Yang *et al.* developed a high-throughput inkjet printing strategy for fabricating chiral structural-color graphics using polymerizable liquid crystal inks (Fig. 6e–g).[114] By leveraging evaporation-induced self-assembly dynamics of liquid crystal inks, the team achieved high-resolution, angle-dependent structural colors with resolutions exceeding 72 dpi on diverse substrates, including glass, silicon wafers, metals, and flexible textiles. Precise control over helical nanostructures—achieved *via* reactive mesogens, chiral dopants, and chain extenders—yielded multi-colored circularly polarized photonic graphics, advancing anti-counterfeiting and interactive display technologies.

Unlike traditional structural colors that depend on periodic arrangements of photonic structure units, a novel coloration mechanism based on TIR and interference was introduced in 2019 by Zarzar's group.[115] This approach eliminates the need for periodic nanostructures, enabling brilliant colors from individual microscale concave interfaces. Furthermore, Song's group developed an inkjet-printing strategy to rapidly fabricate dome-shaped microstructures (microdomes) for generating structural colors based on TIR and interference (Fig. 6h–k).[116] By controlling droplet volume and substrate wettability, they achieved full-color printing with a single transparent ink, covering 72% of the standard Red Green Blue (sRGB) color gamut. The pixelated microdomes allowed grayscale tuning (0.152–0.803) and high-resolution imaging (up to 842 dpi), producing photorealistic portraits and functional patterns like QR codes. Notably, the optical Janus effect-color on one side, and transparency on the other-expanded applications in static displays (*e.g.*, anti-counterfeiting labels) without requiring dynamic stimuli.

Moreover, dielectric- and metal-based metasurfaces/metamaterials have emerged as important platforms for reflective displays due to their high resolution.[117–120] For instance, Yang *et al.* demonstrated an all-dielectric Si metasurface integrated with a refractive index matching layer, achieving record color gamuts exceeding 180% sRGB (Fig. 7a and b).[121] By leveraging the interplay between electric and magnetic dipole resonances, this design significantly suppressed broadband background reflection and narrowed full width at half maximum (FWHM), enabling high-brightness, high-purity structural colors. Moreover, Sahu *et al.* demonstrated a single-step thermal evaporation process to fabricate liquid gallium nanoparticles embedded in PDMS, where capillary interactions between uncrosslinked oligomers and Ga vapor drove the self-organization of plasmonic nanostructures (Fig. 7c and d).[122] By tuning the PDMS oligomer content and deposition parameters, the Ga nanodroplets formed multi-layered configurations with controlled size distributions, enabling various structural colors *via* localized surface plasmon resonances. These resonances spanned a broad CIE gamut, with chromaticity modulated by the interplay of inter- and intra-layer gap plasmons. The technique achieved scalable patterning of structural colors over large areas through substrate-selective deposition. Encapsulation with PDMS superstrates further ensured environmental stability against humidity, temperature, and mechanical wear, making the platform viable for outdoor signage and durable decorative surfaces. Moreover, Geng *et al.* utilized femtosecond lasers to induce oxidation in TiAlN–TiN hybrid films, generating structural colors with 90% sRGB gamut and over 10 000 dpi resolution (Fig. 7e and f).[123] The double-resonance absorption mechanism, arising from non-trivial

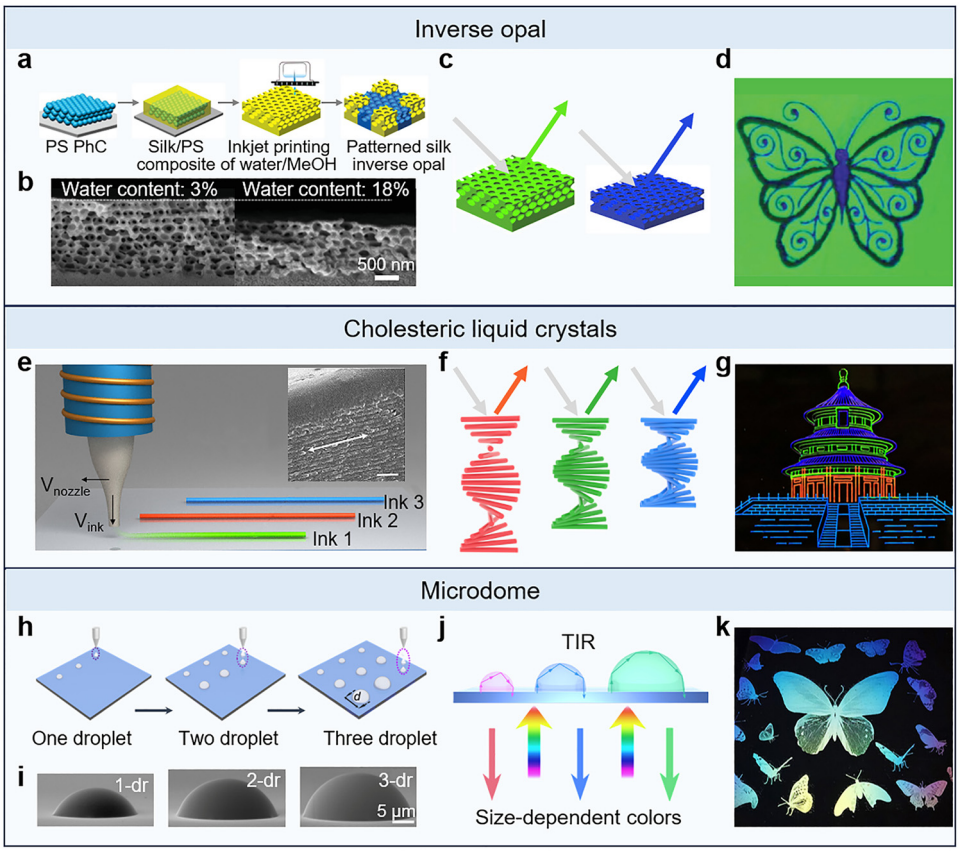

Fig. 6 Structural color imaging based on PhCs or microdomes. (a) Fabrication of a colorful image based on an inverse opal PhC structure. (b) Representative SEM images of inverse opal PhC with different colors. (c) Schematic of the interaction between the inverse opal structure and light. (d) Pixelated image based on inverse opal PhC structure. Reproduced from ref. 113 with permission from John Wiley and Sons, copyright 2019. (e) Schematic of direct ink writing blue, red, and green lines based on cholesteric liquid crystal structure. Inset is the cross-sectional SEM image of the printed green line. (f) Schematic of the interaction between cholesteric liquid crystals (CLCs) and light. (g) Temple of Heaven pattern based on CLCs. Reproduced from ref. 114 with permission from Elsevier, copyright 2024. (h) Schematic illustration of the droplet-by-droplet printing to create microdomes with different diameters. (i) SEM image of printed microdome structure with different diameters. (j) Schematic of the interaction between microdome and light. (k) The large-area color image based on microdomes. Reproduced from ref. 116 with permission from American Association for the Advancement of Science, copyright 2021.

phase shifts at the oxide-TiAlN interface and TiAlN–TiN interface, enabled high-throughput inkless printing on rough and flexible substrates. The laser-oxidized films demonstrated exceptional fastness against UV, corrosion, and abrasion, surpassing traditional plasmonic colorants in durability. This non-contact, single-step fabrication circumvents the cost and complexity of e-beam lithography, paving the way for its industrial adoption in decorative and security printing.

3.1.2 Dynamic display. Inspired by the dynamic coloration mechanisms in nature, advanced photonic systems have emerged as transformative platforms for next-generation displays by integrating stimuli-responsive materials with micro-nano structures.[124–126] The generation of structural color is related to micro-nano structures, so the dynamic regulation of structural color can be realized by changing the period, size, orientation, or refractive index of micro-nano structure. For example, Ge's group demonstrated an electric-field-responsive colloidal PhC that achieves full-color dynamic displays by modulating the interparticle distance of SiO_2 particles (Fig. 8a).[127] This metastable PhC, formed by supersaturation-induced self-assembly in a mixture of propylene carbonate and trimethylolpropane ethoxylate triacrylate, exhibits reversible assembly and disassembly behavior. By applying different voltages, the Bragg reflection peak shifts due to changes in particle spacing (period), enabling color tuning across the visible spectrum. Subsequently, Ge's group developed a series of electric-field-responsive colloidal PhC systems featuring enhanced performance through nanoparticle-modified electrodes,[128] solvent optimization,[129] and region-selective electrode design.[130] These innovations enabled low-voltage actuation, high color saturation, multilevel response, and gradient display effects, offering new strategies for energy-efficient displays and dynamic anti-counterfeiting labels. In addition, Miller *et al.* developed a dynamic structural color material based on mechanical deformation, leveraging an adapted Lippmann photography technique.[131] Commercial photosensitive elastomers are used to record periodic refractive index variations *via* digital projection. When subjected to stretching

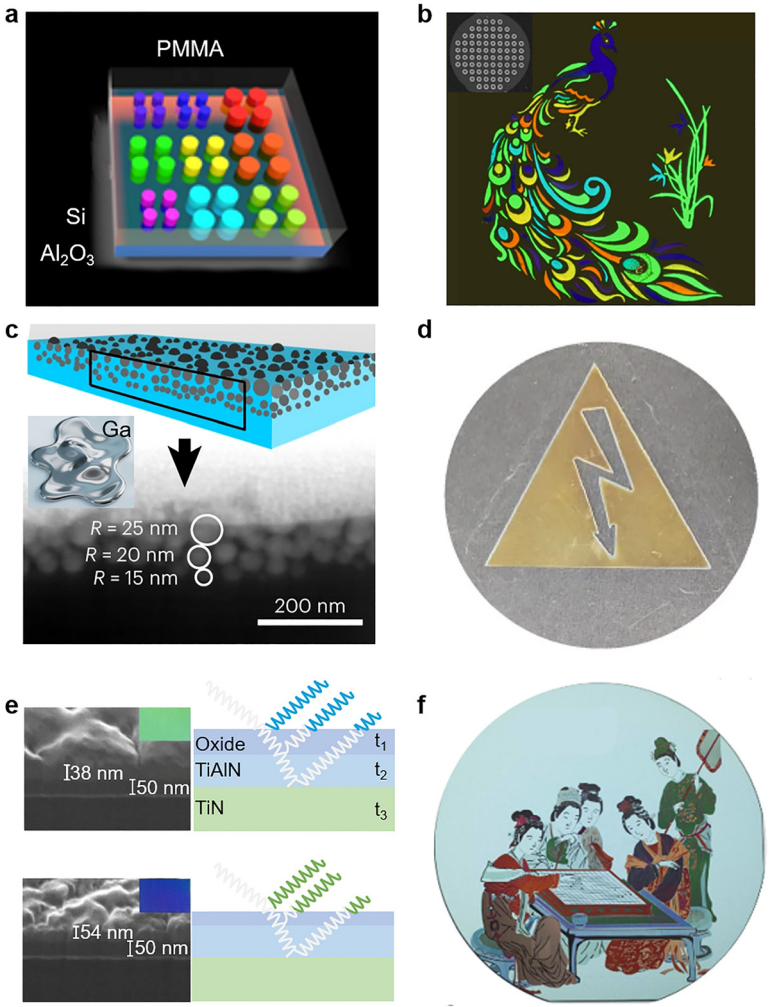

Fig. 7 Structural color imaging based on metasurface or metamaterials. (a) and (b) Full-color image printing with Si metasurface. Reproduced from ref. 121 with permission from Springer Nature, copyright 2020. (c) and (d) Image based on Ga-deposited nanoparticles. Reproduced from ref. 122 with permission from Springer Nature, copyright 2024. (e) and (f) Large-scale structural color patterns printed on TiAlN–TiN hybrid films on a polished 2-in. Si wafer. Reproduced from ref. 123 with permission from Springer Nature, copyright 2023.

or compression, the period of the photonic structures changes, resulting in a shift in the reflection peak wavelength. This material maintains stability over thousands of deformation cycles, making it suitable for wearable devices and health monitoring applications. Moreover, for photonic structures that do not require a periodic arrangement, changing the size of an individual structure can also alter its structural color. For instance, Li *et al.* demonstrated a dynamic structural-color display strategy by leveraging non-periodic microdome arrays fabricated from humidity-responsive polyacrylic acid hydrogels (Fig. 8b).[38] In their approach, inkjet-printed microdomes with precisely controlled size exhibit total TIR-based structural colors, which dynamically shift across the visible spectrum under varying relative humidity (RH). As RH increases, hydrophilic microdomes absorb moisture and swell, altering their size. This geometric modulation changes the light reflection paths within the microdomes, inducing full-spectrum color transitions from red to blue. Besides altering period and size, changing the orientation of photonic structures can also achieve color change. Hou *et al.* proposed a strategy to adjust the structural color by controlling the orientation of 1D diffraction grating through the topological deformation of kirigami structure (Fig. 8c).[132] This design uses the azimuth dependence of diffracted light from 1D grating to realize high contrast optical switching (color on and off), thus realizing a dynamic display. When integrated with dielectric elastomer actuators, the platform achieves 15 000-cycle durability, demonstrating robust potential for mechanically adaptive displays. Moreover, tuning the refractive index of the building blocks or the surrounding matrix in photonic structures provides an alternative strategy for dynamic structural color displays. This modulation typically involves physicochemical mechanisms such as thermally driven phase transitions, electric field-mediated liquid crystal reorientation, or the introduction of new substances. Franklin *et al.* presented a tunable color system by coupling high birefringence liquid crystals with

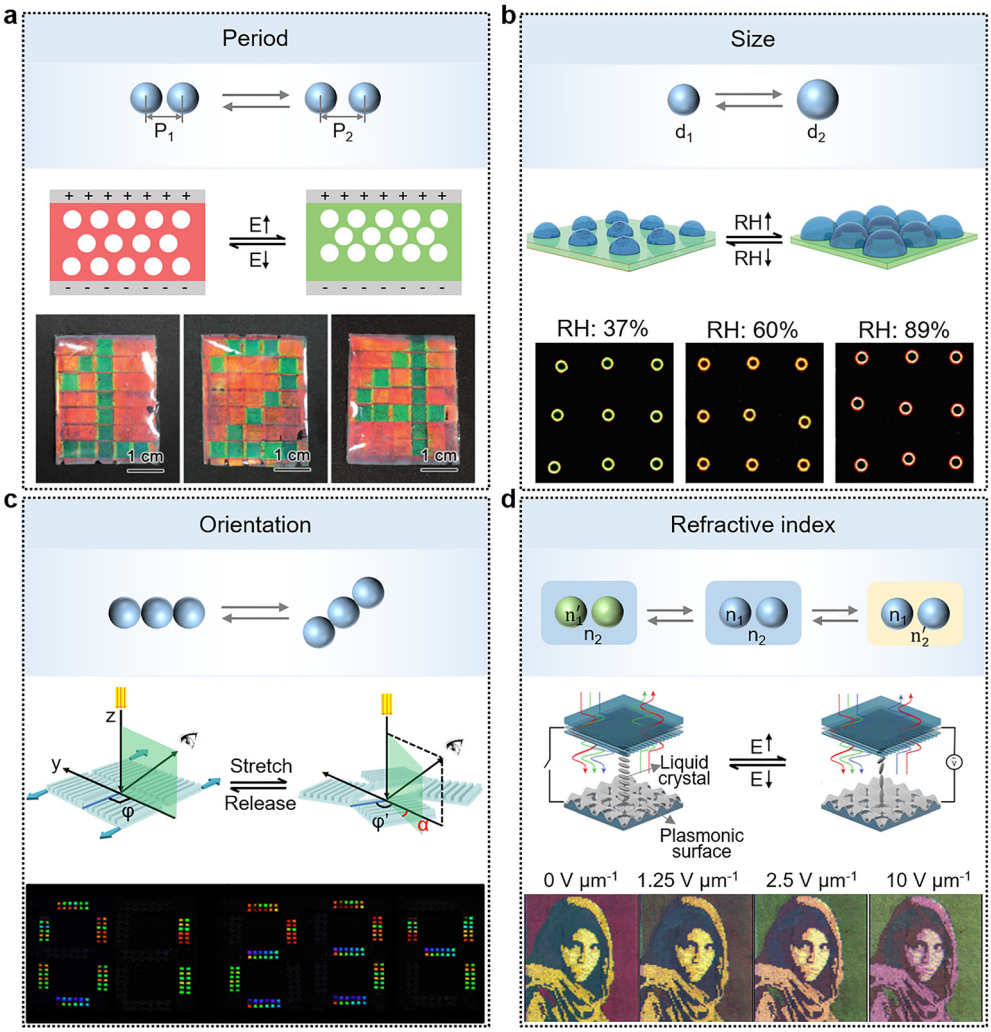

Fig. 8 The applications of micro/nano photonic materials in dynamic display. (a) Dynamic display based on the change of PhC period. Reproduced from ref. 127 with permission from Wiley-VCH Verlag GmbH & Co. KGaA, Weinheim, copyright 2017. (b) Dynamic display based on the change of microdome size. Reproduced from ref. 38 with permission from Wiley-VCH GmbH, copyright 2024. (c) Dynamic display based on the change of grating orientation. Reproduced from ref. 132 with permission from Science China Press, copyright 2023. (d) Dynamic display based on the change of refractive index. Reproduced from ref. 133 with permission from Macmillan Publishers Limited, copyright 2015.

plasmonic surfaces (Fig. 8d).[133] Voltage-induced reorientation of liquid crystal molecules alters the refractive index surrounding the plasmonic surface, leading to full-color coverage across the visible spectrum.

3.2 Information encryption

Micro/nano photonic materials have emerged as powerful platforms for advanced information encryption due to their unique ability to manipulate light–matter interactions at subwavelength scales.[134–137] Unlike conventional encryption methods relying on digital algorithms, photonic encryption leverages the multidimensional degrees of freedom (DoFs) of light—such as wavelength, polarization, amplitude, phase, and propagation direction—to achieve high-capacity and high-level security features. Bioinspired designs further enhance these systems by mimicking natural structural coloration and optical phenomena observed in butterflies, beetles, and other organisms. It offers a versatile toolkit for information security, spanning static multiplexing of light's DoFs and dynamic stimuli-responsive encryption. This section categorizes photonic encryption strategies into two ways: (1) static systems where information is multiplexed by controlling optical DoFs without structural changes, and (2) dynamic systems combining tunable structural colors or fluorescence with external stimuli (*e.g.*, strain, humidity).

3.2.1 Multiplexed information encryption. Light possesses multiple DoFs, such as wavelength, intensity, polarization, and angular momentum, and each DoF can be used as a channel for information encryption.[138–140] Advanced photonic structures allow structural design to manipulate multiple DoFs of light simultaneously, thereby enabling multidimensional and multichannel information encryption with enhanced security (Fig. 9).[141–144] Metasurface/metamaterial is a powerful candidate for multichannel information encryption platform because of its

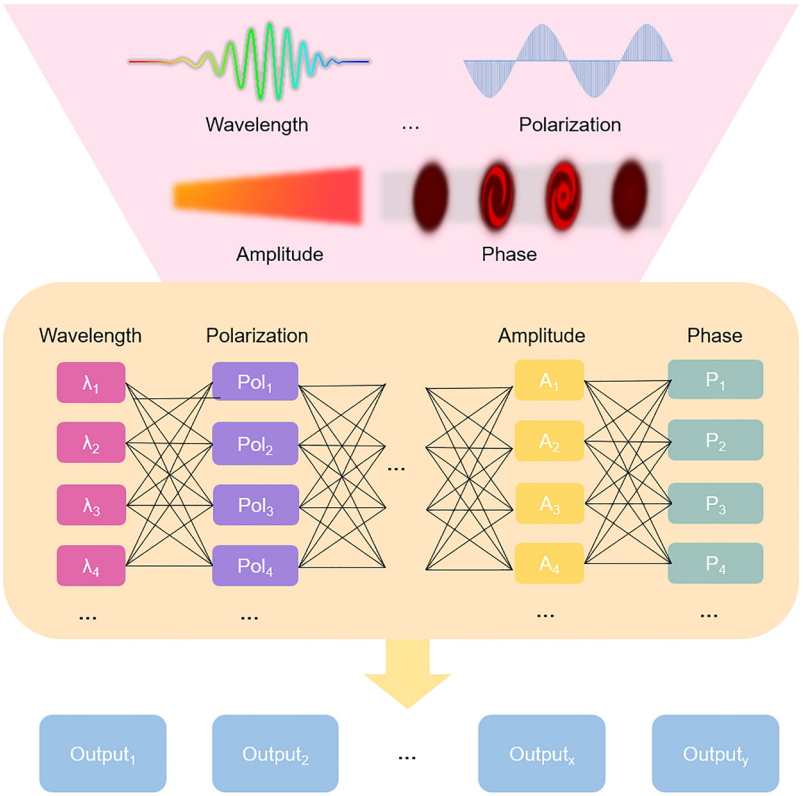

Fig. 9 Multiple DoFs of light as input for multi-channel information encryption and storage.

excellent ability to manipulate the DoFs of electromagnetic waves.[145–148] For example, Zhao *et al.* pioneered a diffraction-order decoupling strategy in metasurfaces by analyzing phase correlations across diffraction channels (Fig. 10a–c).[149] Their single-cell design synergizes detour phase and Pancharatnam–Berry (PB) phase modulation, enabling independent control of four optical DoFs—wavelength (480/532 nm), wavevector direction (*x*/*y*-axis), polarization (LCP/RCP), and diffraction order (−1st/−3rd)—to generate 16-channel metahologram. This multidimensional encryption system elevates decryption complexity by orders of magnitude, making it promising for advanced anti-counterfeiting. However, challenges persist in metasurface/metamaterial scalability due to the complex fabrication process and high cost. To address these limitations, Li's group fabricated quasi-3D PhC composite films (PCCFs) *via* self-assembly and nanoimprinting (Fig. 10d–f).[150] The PCCFs consists of a 2D PhC of a closely packed monolayer of polystyrene spheres (600 nm period) containing a periodic array of microshallow pits (2.5 μm period), enabling simultaneous control over scattering, diffraction, and polarization. Recently, they also found a chiral structural color from microdomes, which is related to the phase delays caused by TIRs (Fig. 10g and h).[151] This microdome structure can not only regulate the wavelength and intensity of light, but also regulate the phase and polarization, enabling multichannel encryption. The chirality, tunable across visible wavelengths, achieves 2^{32} cryptograms when patterned as concentric arcs on contact lenses.

3.2.2 Information encryption based on external stimuli. Stimuli-responsive photonic materials exhibiting dynamic structural modulation have emerged as a sophisticated platform for multichannel information encryption.[152–154] For example, Xue *et al.* demonstrated a bioinspired encryption strategy by fabricating gradient-crosslinked hydrogel microdomes *via* oxygen-inhibited photopolymerization (Fig. 11a and b).[155] The solvent-responsive structural color of each microdome, arising from total internal reflection and interference, is dynamically tuned by controlling UV curing time and sequential solvent development (*e.g.*, water and ethanol). Microdomes with gradient crosslinking degrees exhibit programmable color shifts under specific solvents, enabling pixel-level integration of multiple information states. Integrating ASCII-based algorithm cryptography, the system assigns duodecimal codes to solvent-etched geometric symbols, where decryption requires both the correct solvent sequence (keys) and predefined coding rules. This dual-layer security ensures that attackers must simultaneously possess the physical solvent keys and algorithmic mappings to access valid data, significantly elevating anti-counterfeiting complexity. The approach merges scalable fabrication with high-density optical storage, offering broad potential for secure labeling and confidential data encryption. Beyond solvent response, mechanochromic elastomers also offer unique advantages in dynamic encryption, which can rapidly and repeatedly switch different structural color patterns by applying mechanical stress. As for these elastomer-based materials, a new coloration mechanism was proved by Ruan

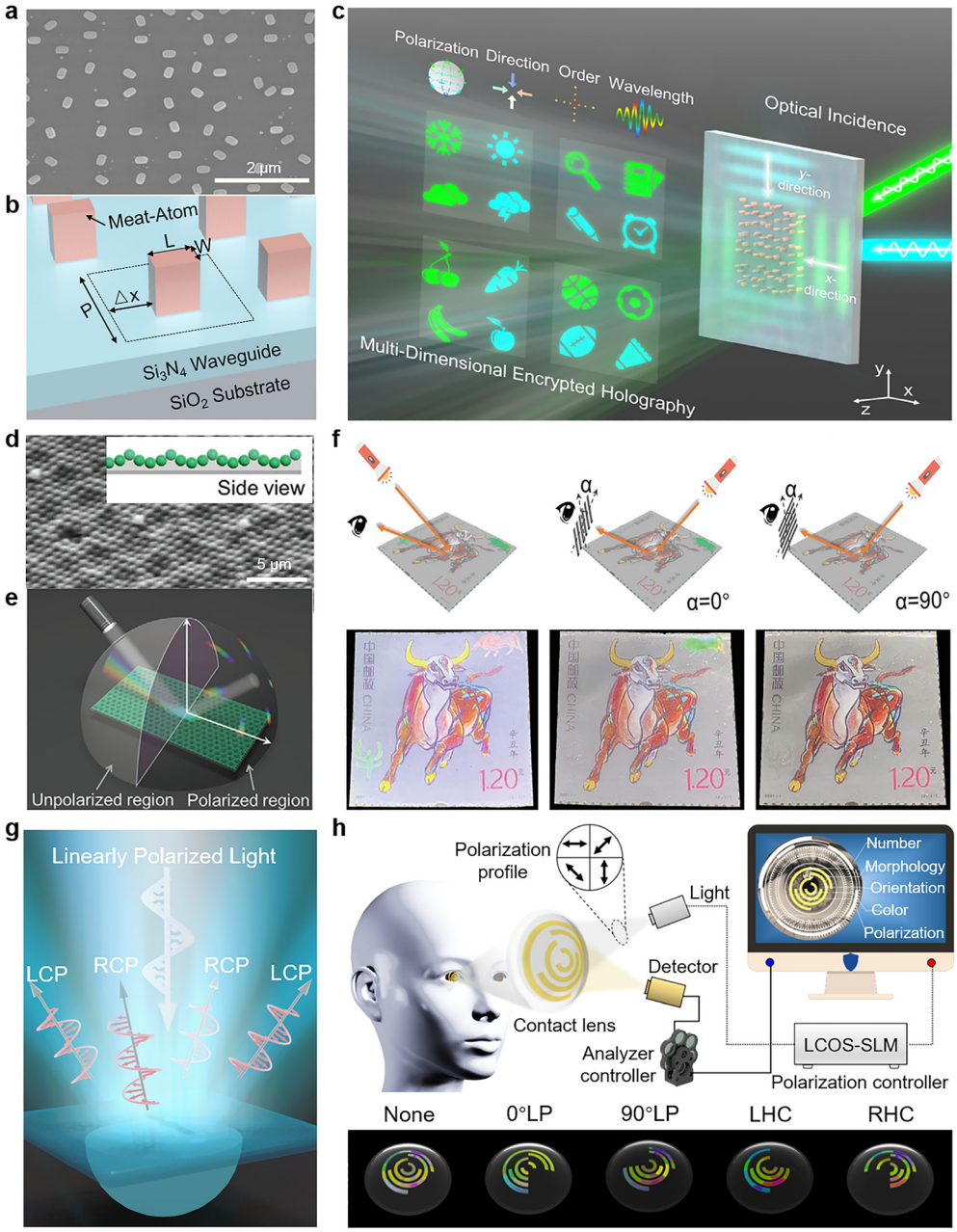

Fig. 10 Multichannel information encryption based on multidimensional regulation of light by optical structure. (a)–(c) Multidimensional encrypted *meta*-optics storage based on order-decoupled metasurface. Reproduced from ref. 149 with permission from Wiley-VCH GmbH, copyright 2025. (d)–(f) Multichannel image switching based on polarization-sensitive PhC composite film. Reproduced from ref. 150 with permission from Wiley-VCH GmbH, copyright 2022. (g) and (h) Contact lenses integrated with chiral-structural-color microdomes for identity authentication. Reproduced from ref. 151 with permission from the National Academy of Sciences, USA, copyright 2025.

et al. that individual trench could generate a specific color due to variations in trench depth and switch multiple colors by directional strains and capillary forces, as shown in Fig. 11c and d.[156] Relying on the outstanding stretchability of PDMS, the reversible modulation of the shapes and structural colors of the aforementioned structure could be achieved. A variety of information can be hidden in a PDMS relief composed of trenches with different structural parameters. As an instance, a blue "F3" pattern was shown by the capillary force, and a "1" and an "A3" pattern were revealed following the synthetic operation of imposing *x*/*y* strain and release, respectively. Furthermore, the higher security often requires combining multiple optical phenomena, such as structural color, fluorescence, or phosphorescence. Huang *et al.* mimicked Troides magellanus butterfly wings by integrating luminescent lanthanides (chemical units) with colloidal PhCs (physical units) (Fig. 11e–g).[157] The as-prepared PhC films prepared by molecule-mediated shear-induced assembly technique (MSAT)

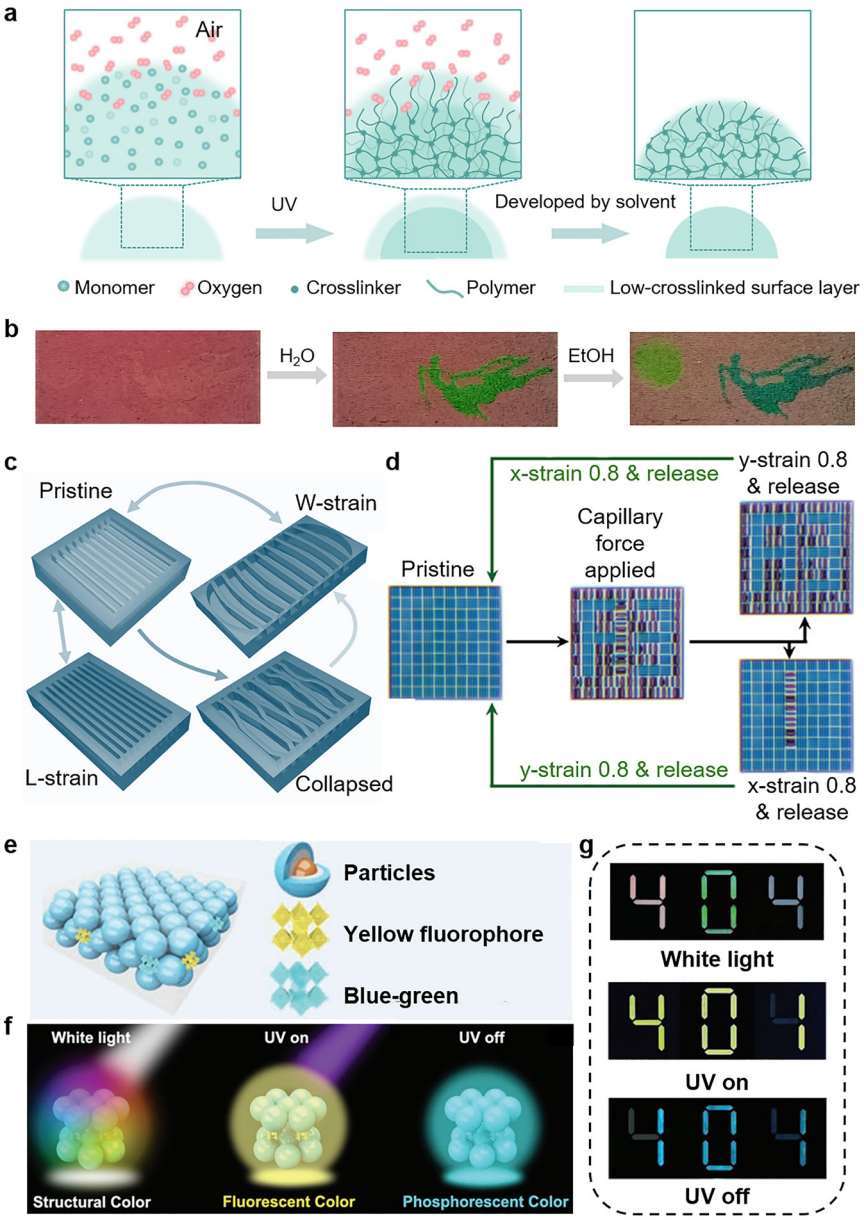

Fig. 11 Multichannel information encryption based on responsive materials. (a) and (b) Solvent responsive information encryption based on Gradient-crosslinked hydrogel microdome pattern. Reproduced from ref. 155 with permission from Science China Press, copyright 2023. (c) and (d) Schematic diagram of PDMS trenches with multiple sets of encoding information. With directional strains, the width and length of trenches can be changed, and capillary force collapsed the structure. Under appropriate conditions, hidden information will be revealed. Reproduced from ref. 156 with permission from Wiley-VCH GmbH, copyright 2021. (e)–(g) Tri-state PhC film for multilevel information encryption enabled by both physical and chemical structures. Reproduced from ref. 157 with permission from Wiley-VCH GmbH, copyright 2023.

feature three optical states: structural color under white light, fluorescence under UV, and phosphorescence in darkness. By patterning different lanthanides into distinct regions, a single film carries triple-encrypted information decipherable only with specific light sources.

3.3 Optical sensors

Natural biological optical systems rely on the precise design of microstructures rather than chemical dyes, offering profound insights for the development of artificial optical sensors. Biomimetic micro- and nano-optical structures for sensing have long been a hot topic of research. Sensors with fine structural design rely on sub-wavelength scale optical field localization and light–matter interactions to respond to external stimuli (including physical (light, heat, humidity, *etc.*), chemical (pH, VOC gas, *etc.*), and biological) in a label-free, real-time, highly sensitive, and visual way. People are fascinated with the convenience of naked eye sensors. In this chapter, we will focus on visualizing and miniaturizing bionic optical sensors.

PhCs as a typical photonic structure are always the most famous carriers for visual sensing. The use of PhCs to detect external stimuli with the naked eye is a research hotspot. The sensing mechanisms can be broadly categorized into two aspects: one is the variation of structural parameters and the other is the manipulation of the optical field. PhCs are composed of periodically arranged materials, and their optical properties are highly dependent on structural parameters (lattice spacing, porosity, refractive index contrast, *etc.*). When external stimuli (*e.g.*, temperature, humidity, pressure, chemical substances) lead to deformation, expansion, or reorganization of the PhC structural units, their photonic band gap positions are shifted, which in turn causes structural color changes visible to the naked eye. By establishing a quantitative relationship between the structure color and the parameter to be measured, visual sensing can be realized. Inspired by this iridescent color-changing principle, there exists a vast body of remarkable literature. For example, Zhao *et al.* proposed a novel structural color microneedle patches (EMNs) composed of PhCs and microneedle arrays to *in situ* detect multiple wound biomarkers (Fig. 12a).[158] The EMNs were divided into different regions for the detection of distinct small molecules. By selecting specific stimulative response materials, the presence of target molecules can create responsive volume change, resulting in a change in structural color. As a demonstration, they chose the wound as the inspection object (Fig. 12b). Notably, for pH detection, the bacterial infection group exhibited a red-shifted color compared to the other two groups. For glucose detection, the diabetes group showed a redder color than the other two groups.

Beyond common colloidal PhC structure colors, CLCs, as a unique type of PhC, form helical superstructures through the self-assembly of chiral supramolecules, which is popular in fabricating sensors.[159] These structures can selectively reflect circularly polarized light at specific wavelengths, exhibiting dynamically tunable structural colors. With significant optical responsiveness to external stimuli such as temperature, light, and electric fields, CLCs demonstrate rapid response speeds, excellent reversibility, and outstanding processing flexibility. These characteristics have established them as a

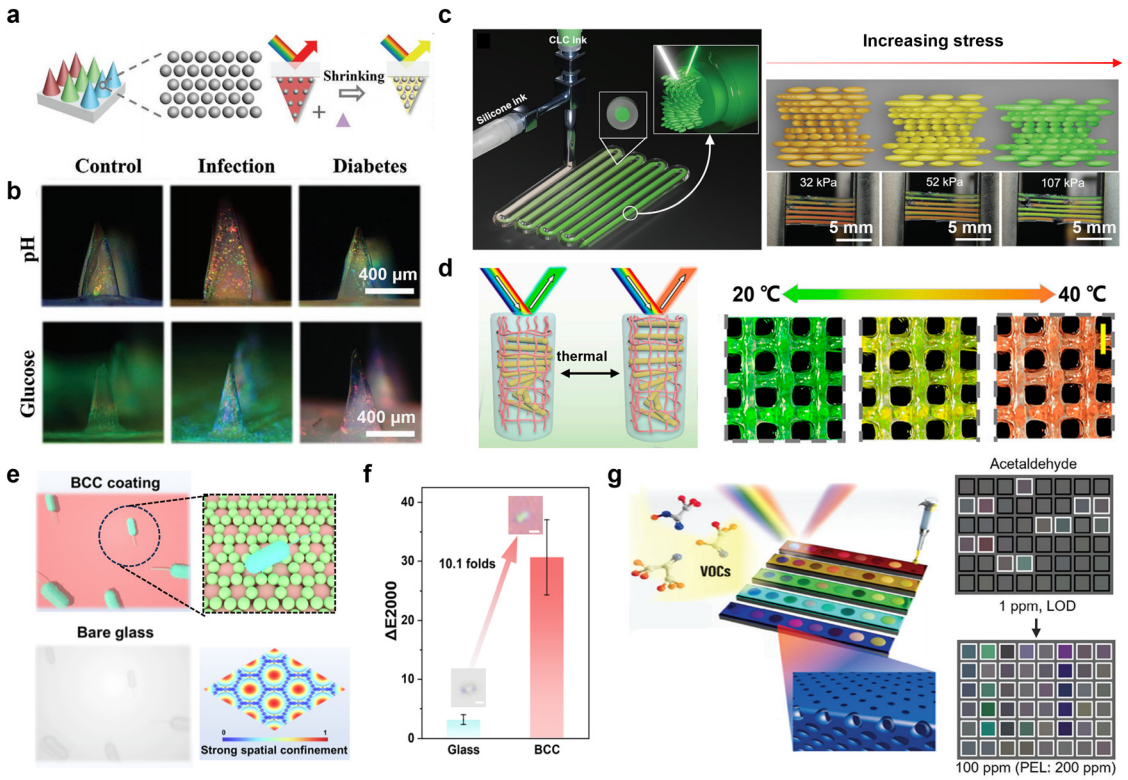

Fig. 12 Bioinspired visual optical sensors based on different working principles. (a) and (b) Schematic illustration of the sensing mechanism of small molecule detection of the EMNs. Target molecules cause changes in EMNs' volume, leading to a vivid visual color change. *In vivo* detection of EMNs for pH and glucose detection. Reproduced from ref. 158 with permission from Wiley-VCH GmbH, copyright 2023. (c) Schematic of the setup of coaxial 3D printing and illustration of the CLC tensile sensor change in the pitch length under uniaxial tension and the corresponding optical images. Reproduced from ref. 160 with permission from Wiley-VCH GmbH, copyright 2025. (d) Schematic illustration of the thermally responsive color variation property of objects based on cholesteric cellulose liquid crystal. Optical images of an object showing color variations under different temperatures. Reproduced from ref. 161 with permission from National Academy of Sciences, USA, copyright 2022. (e) and (f) Color contrasts of bacteria in the BCC-coated glass slide and bare glass can be improved 10.1-fold. Near-field analysis of BCCs indicates strong spatial confinement of light. Reproduced from ref. 162 with permission from American Chemical Society, copyright 2025. (g) Schematic of colorimetric sensor array relying on dye-cPhC. Detecting acetaldehyde at 1 ppm (limit of detection) and 100 ppm (permissible exposure limit) with pronounced color changes. Reproduced from ref. 163 with permission from Wiley-VCH GmbH, copyright 2024.

"star performer" widely employed in smart sensing and dynamic optical devices, making them a prominent material in cutting-edge photonic applications. Yang *et al.* successfully fabricated cholesteric liquid crystal elastomers *via* direct ink writing with prominent mechanochromic properties (Fig. 12c).[160] They attempted to utilize two inks for coaxial printing: CLC ink as the core material and transparent silicone ink as the shell material. Using this method, the core can be supported by the silicone shell, meanwhile enabling the cholesteric phase to rapidly self-assemble. The mechanochromic properties of the sample were characterized. As can be seen, the sample showed a blue shift in color when tensile stress was applied. Because lateral compression accompanying uniaxial tension reversibly compresses the pitch, resulting in the blue shift. The mechanochromic sensitivity of the printed sample is higher than that of bare CLC. It should be noted that the blue shift in color can be reversible for at least 100 cycles under 20% strain. Combining parameter-sensitive structures with stimulative responsive materials, researchers have designed various types of sensors. Another similar but classic example was done by Zhao's group.[161] They achieved a printable structural color material relying on cholesteric cellulose liquid crystals mixing with gelatin and a thermal-responsive hydrogel (Fig. 12d). Both of these filling substances have brilliant thermal responsiveness. Thus, the helical pitch could be modulated under the control of environmental temperature leading to color tunability. It exhibited a pronounced color change from green to red in the range of 20–40 °C.

PhCs have many intriguing optical functions, including the aforementioned tunable structural color and the regulation of optical fields. There are enormous papers about the latter in the sensing field. In general, slow light effect or increasing local optical density enhances light–matter interactions and the modulation of spontaneous radiation efficiency (Purcell effect) can extremely boost the detection signal when the fluorescence emission peak overlaps with the PhC bandgap edge. Based on these basic mechanisms, some novel ideas are emerging to improve sensing performance. In a more recent study, inspired by the Brazilian opal, binary colloidal crystals (BCCs) for high-contrast imaging were produced by Song *et al.* (Fig. 12e).[162] It is a unique structure unlike traditional PhCs, which consist of two distinct nanoparticles. Compared to bare glass, the BCCs can improve color contrasts by an order of magnitude (Fig. 12f). As the figures show, the same undyed bacteria is difficult to identify with a commercial optical microscope because of the weak scattering signals. But it can be seen easily in cyan colors using the red BCCs substrate. Near-field analysis of BCCs gives us the reason for high-contrast Imaging. The scattering signals are remarkably amplified by taking advantage of the strong resonance-induced spatial confinement effect.

In addition, unlike the common principle of modulating the rate of spontaneous radiation to enhance the fluorescent signal, Yang and coworkers mentioned a new type of design combining absorption dyes and PhCs to construct a dye-cPhC colorimetric sensor array (Fig. 12g).[163] It has been demonstrated that spectral overlap between the dye's absorption peak and the bandgap of cPhCs significantly provides a more noticeable VOC sensing signal. Therefore, cPhCs with broad and multiple reflective peaks were produced through spin-coating to improve the likelihood of overlapping with dyes. As a preliminary validation, they constructed a 5 × 8 array, a total of 40 spots to test the detection performance for acetaldehyde, acetone, and acetic acid. Taking acetaldehyde as an instance, the color change was observed at 1 ppm and became more and more pronounced with increasing concentration. The sensor array can distinguish acetaldehyde, acetone, and acetic acid with enhanced sensitivity.

In conclusion, bionic micro-nano optical structures provide a revolutionary solution for optical sensing technology with high performance and miniaturization. With the cross-fertilization of nanotechnology, smart materials, and artificial intelligence, this field is gradually moving towards major application scenarios such as clinical diagnosis, becoming the core driving force of next-generation optical sensing technologies.

3.4 Thermal management

Engineered micro-nano photonic structures are revolutionizing radiative cooling technologies, establishing themselves as indispensable platforms for next-generation thermal management.[164–166] By decoding biological mechanisms of organisms from extreme environments, these materials achieve sub-ambient cooling through multiscale structural hierarchies that synergistically manipulate photon transport and phonon scattering.[167,168] Their engineered spectral selectivity enables simultaneous high solar reflectance (>95%) and mid-infrared emissivity (>90%), while adaptive interfacial architectures allow real-time thermal modulation in response to environmental stimuli.[169] Such breakthroughs are redefining sustainability paradigms across scales—from zero-energy building climatization to spacecraft thermal shields—by converting waste heat into radiative power flows through the atmospheric transparency window (8–13 μm), ultimately bridging photonic innovation with global carbon neutrality imperatives.[170]

In harsh environments, organisms have evolved sophisticated optical strategies to manage thermal loads. A quintessential example is the Saharan silver ant (*Cataglyphis bombycina*), which survives desert surface temperatures exceeding 60 °C through a dual-functional hair structure (Fig. 13a–e).[171] These triangular, micrometer-scale hairs enhance solar reflectance (67% in visible and near-infrared (NIR) wavelengths) *via* Mie scattering and total internal reflection while simultaneously boosting mid-infrared emissivity for radiative heat dissipation. This biological solution enables the ants to maintain body temperatures below 53.6 °C during peak solar exposure. Such mechanisms highlight nature's ability to decouple optical properties across spectral bands-a principle that has inspired the design of artificial radiative coolers.

Building on these biological insights, researchers have developed inorganic materials that replicate natural thermal regulation strategies.[172] Lin *et al.* engineered a hierarchically porous ceramic inspired by the *Cyphochilus* beetle's ultra-white

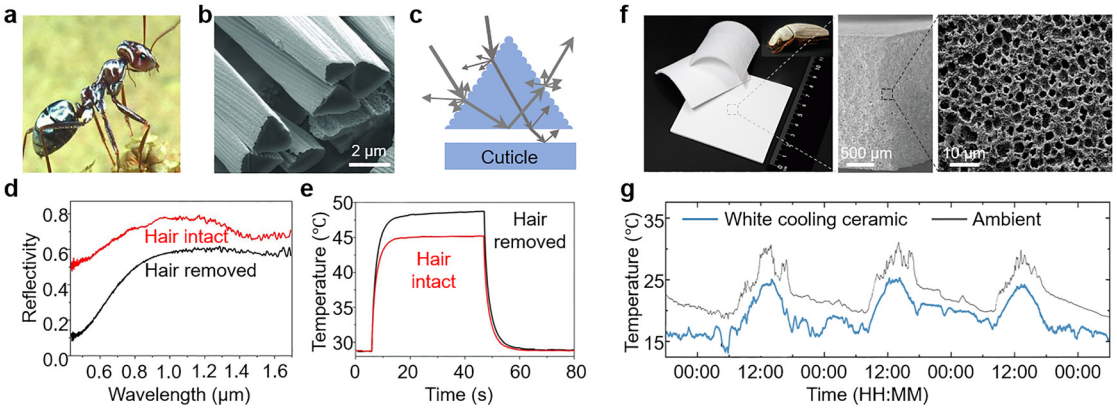

Fig. 13 Passive radiative cooling based on optical structure. (a)–(e) Structure and cooling mechanism of silver ant hair. Reproduced from ref. 171 with permission from AAAS, copyright 2015. (f) and (g) Cooling ceramics with a hierarchically porous structure. Reproduced from ref. 173 with permission from AAAS, copyright 2023.

scales (Fig. 13f and g).[173] The ceramic with a multidispersed pore system achieves a near-perfect solar reflectivity of 99.6% and high mid-infrared emissivity (96.5%). The cooling ceramic enables an average subambient temperature reduction of 4.3 °C during the daytime. However, while such high-reflectance materials excel in cooling efficiency, their monotonous white appearance limits aesthetic integration in urban and architectural contexts.

To address this limitation, color layers like pigment color,[174,175] photoluminescence,[176–178] and structural color[179–182] have been introduced in the radiative coolers. For example, Li *et al.* demonstrated a pink-colored radiative cooler employing a seven-layer $Si/SiO_2/TiO_2$ stack. The color comes from Fabry–Pérot resonator (Fig. 14a and b).[183] By designing photonic structures with tailored absorption in the visible range and high reflectance in the NIR, they achieved pink-colored surfaces that were 22.6 °C cooler than conventional paints under identical solar exposure.

However, the introduction of absorption-based colorants, such as pigments/dyes, photoluminescent materials, and resonant absorption structures, in radiative coolers inevitably results in absorption across the solar spectrum, which reduces the cooling performance.[184] To solve these problems, Hou *et al.* developed a bioinspired radiative cooling film mimicking the hierarchical structure of scarab beetle elytra (Fig. 14c and d).[185] Their design integrates close-packed colloidal PhC hemispheres within a porous polymethyl methacrylate (PMMA) substrate, achieving 93.4% solar reflectance and 92.3% atmospheric window emissivity. This colorful cooling film can realize subambient cooling of ~10.2 °C at night and ~7.2 °C at midday. The simple nesting of a colorful coating in surface pits can preserve its subambient cooling performance and provide an appealing aesthetic option. This approach bridges the gap between aesthetics and performance, offering a scalable

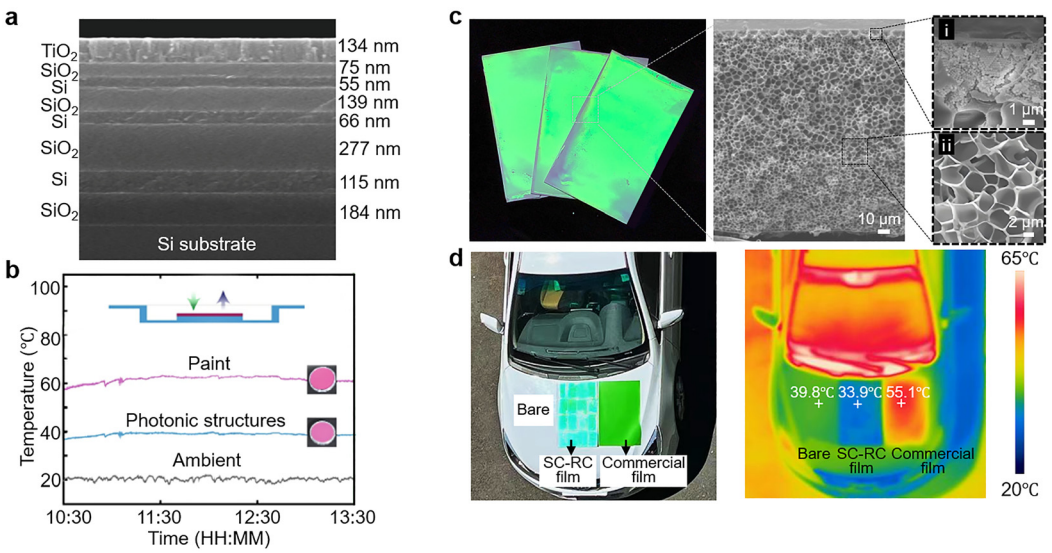

Fig. 14 Colorful passive radiative cooling coating. (a) and (b) Colored radiative coolers based on multilayer photonic structures. Reproduced from ref. 183 with permission from Springer Nature, copyright 2018. (c) and (d) Bioinspired colorful daytime radiative cooling film based on a hierarchically porous nested structure. Reproduced from ref. 185 with permission from Elsevier, copyright 2024.

solution for applications requiring both visual appeal and thermal efficiency.

In addition, PhC films have emerged as promising candidates for smart window applications in thermal management. Inspired by reptiles such as geckos that combine structural and pigmentary colors for adaptive camouflage, researchers have integrated thermochromic dyes and electrochromic materials into colloidal PhCs, achieving dual responsiveness to temperature and voltage with adjustable color intensity.[186] More recently, Li *et al.* developed a smart window system by embedding PhCs into a thermoresponsive hydrogel matrix, enabling multicolor switching and enhanced NIR shielding under varying thermal conditions.[187]

3.5 Light management in optoelectronic devices

Light management refers to the process of engineering the interaction between photons and optoelectronic materials/devices at the micro- and nanoscale.[188] This technology plays a crucial role in enhancing the performance of optoelectronic devices such as SCs, photodetectors (PDs), and LEDs.[189,190] Research has demonstrated a strong correlation between device efficiency and structural design, where bioinspired micro-nano structures offer innovative solutions for light-field manipulation. In the fields of SCs and PDs, bioinspired micro/nano structures—including unitary and hierarchical architectures—significantly improve energy conversion efficiency and photoresponse performance through advanced light-trapping mechanisms such as reduced reflection, enhanced scattering, and enhanced optical path length.[45] Additionally, in photodetectors, the incorporation of polarization-sensitive structures, such as grating structures, not only enhances photoelectric responses but also endows the PDs with polarization-sensitive capabilities.[191] Notably, groundbreaking advances in bioinspired vision chips, incorporating structures mimicking human eyes and compound eyes, are reshaping multiple technological domains, including medical diagnostics, artificial intelligence, and autonomous driving.[192,193] For LEDs, bioinspired strategies such as moth-eye antireflective surfaces, PhCs, scattering structures, and optical microcavities effectively address the limitations of total internal reflection, thereby enhancing the light out-coupling efficiency (OCE).[194,195] This section reviews representative applications of bioinspired photonic structures in optoelectronic devices, focusing on three main functional domains: (1) light management in SCs and PDs (Section 3.5.1), (2) bioinspired visual sensing systems (Section 3.5.2), and (3) light management in LEDs (Section 3.5.3). These topics share similar underlying photonic principles discussed above, and their device architectures and performance objectives differ significantly.

3.5.1 Light management in SCs and PDs. Thin-film SCs offer a material-efficient approach for harnessing solar energy, yet their performance is limited by inherent optical constraints. Taking the highly promising perovskite material as an example, the high refractive index and thin nature of perovskite films result in significant light reflection and parasitic losses, ultimately limiting photon absorption and hindering further improvements in power conversion efficiency (PCE). Photonic structures can significantly improve light absorption by facilitating interactions between the structures and incident light. The photonic structures are typically incorporated into the perovskite active layer, electron transport layer (ETL), hole transport layer (HTL), metal electrodes, and substrates.[191] The light management in SCs and PDs typically employs two principal approaches: reducing reflection and enhancing absorption.[190] For antireflection, quarter-wavelength coatings or nanostructured antireflective layers are commonly used. These coatings are usually optimized for a single wavelength under normal light incidence. Absorption enhancement strategies rely on surface texturing and metallic back reflectors to increase the optical path length *via* multiple internal reflections. For example, substrates with random textures can redirect incident sunlight into the plane of the semiconductor, and constructing optoelectronic devices on such substrates can effectively enhance light absorption. Bioinspired micro-nano photonic structures (such as periodic 1D grating structures and 3D nanostructures) have been extensively studied due to their exceptional light-manipulation capabilities.[189] Two distinct light absorption enhancement mechanisms are observed in typical micro-nano structures, depending on their dimensional characteristics. For structures larger than the optical wavelength, the absorption improvement mainly results from light scattering and reflection between features, extending the optical path length and thus enhancing absorption. In contrast, nanostructures with subwavelength dimensions exhibit superior light-trapping performance due to fundamentally different physical mechanisms. Here, we categorize the optical structures employed in SCs and PDs into single structure (Fig. 15a) and composite structure (Fig. 15b) based on their structural configurations.

3.5.1.1 Single structure. Researchers have integrated various types of single micro-nano structures into SCs and PDs, including gratings,[196–200] nanopillars,[201] nanorods,[202,203] nanocones,[189,204] and moth-eye structures (Fig. 15a).[205,206] As a light-absorbing layer in SCs and PDs, the introduction of photonic structures can reduce the mismatch of refractive indices at interfaces, thus enhancing the light-trapping and efficiency of devices. Wang *et al.* innovatively employed commercial optical discs (CDs/DVDs) as templates to construct large-area grating structures on perovskite active layers *via* nanoimprinting technology.[197] They demonstrated that the grating structures can simultaneously enhance both light-harvesting capability and charge collection efficiency in perovskite SCs, providing a novel approach for improving device performance (Fig. 15c). The precisely patterned diffraction gratings (with periods of 0.75 μm for DVD and 1.5 μm for CD structures) effectively reduced optical reflection while prolonging the photon propagation path through multi-order diffraction effects, resulting in significantly improved light-trapping capability. Ultimately, the DVD-derived grating structure boosted the PCE by 18% (from 16.71% to 19.71%) through enhanced photon management and carrier collection optimization (Fig. 15g). Kang *et al.* introduced moth-eye nanostructures into TiO_2 ETL to enhance the light-harvesting efficiency of perovskite SCs (Fig. 15d).[206] These moth-eye structures effectively confine

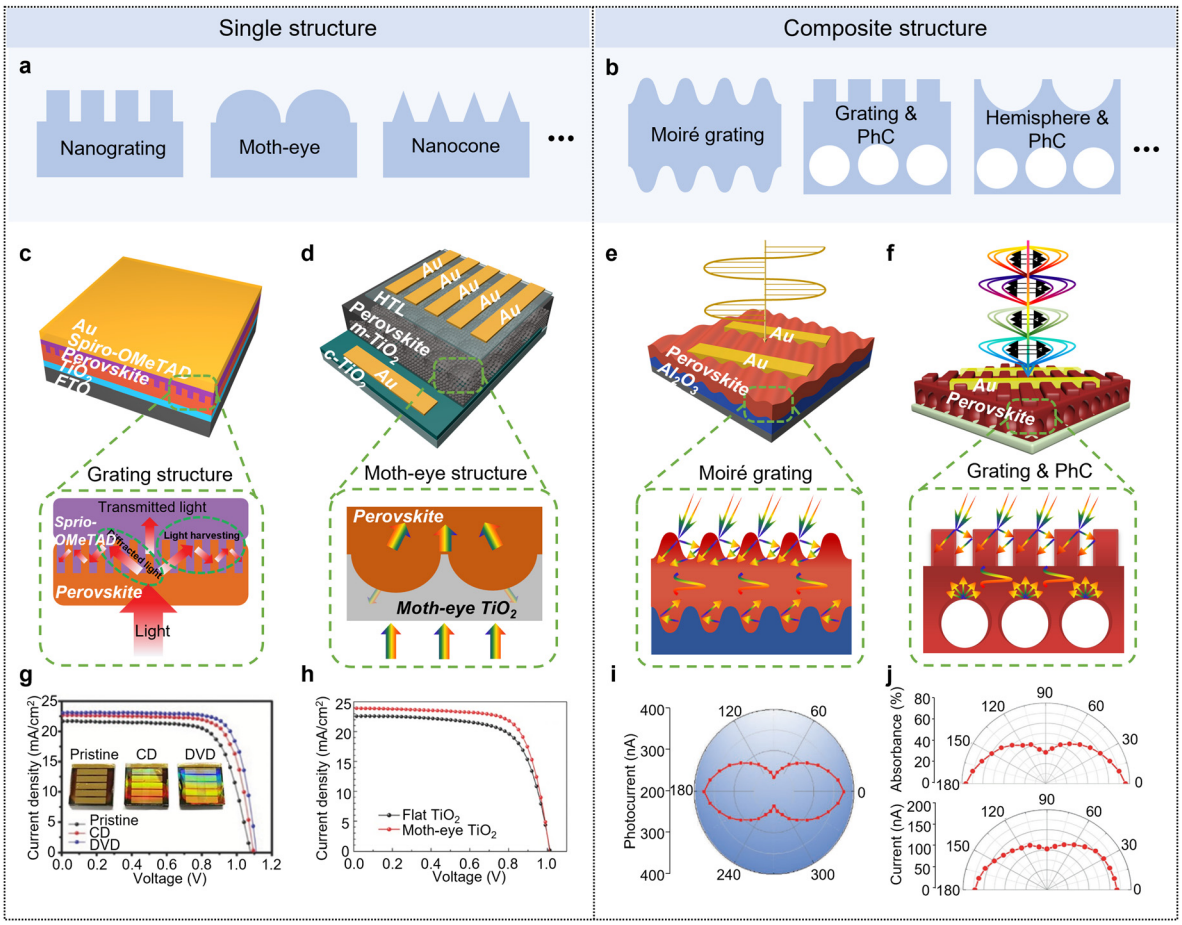

Fig. 15 Light management with single and composite structures in SCs and PDs. Example of light management through (a) single structure and (b) composite structure. (c) Device architecture and light management of the device with grating structure. (g) Influence of grating structure on device performance. Reproduced from ref. 197 with permission from Wiley-VCH Verlag GmbH & Co. KGaA, copyright 2018. (d) Device architecture and light management of the device with moth-eye structure. (h) Influence of moth-eye structure on device performance. Reproduced from ref. 206 with permission from Wiley-VCH Verlag GmbH & Co. KGaA, copyright 2016. (e) Device architecture and light management of moiré perovskite PDs. (i) Polarization response of moiré perovskite PDs. Reproduced from ref. 208 with permission from Wiley-VCH GmbH, copyright 2021. (f) Device architecture and light management of bioinspired perovskite PDs. (j) Polarization-sensitive light detection of bioinspired perovskite PDs. Reproduced from ref. 209 with permission from Wiley-VCH Verlag GmbH &Co. KGaA, copyright 2019.

incident photons within the perovskite active layer through the unique light-management characteristics. The moth-eye structure with a conical shape possesses gradient refractive index properties that efficiently guide incident light into the device while enhancing light absorption in the perovskite film. The moth-eye structure demonstrates superior light-harvesting efficiency across the entire visible spectrum. Ultimately, the perovskite SCs incorporating moth-eye TiO_2 ETL achieved a 10.7% improvement in PCE over their planar counterparts (Fig. 15h). Besides, Wei *et al.* fabricated a moth-eye structure on the [6,6]-phenyl-C_{61}-butyric acid methyl ester (PCBM) ETLs *via* a PDMS template nanoimprinting route.[205] In this configuration, the moth-eye PCBM ETL simultaneously functions as a back electrode, while its PhC characteristics act as a reflective mirror to suppress light leakage, thereby effectively trapping photons within the perovskite active layer for enhanced absorption. They confirmed that this photon structure achieves broadband light absorption enhancement across the entire visible wavelength range. Furthermore, the incorporation of micro-nano structures enables spectrally selective response. Cao *et al.* developed bioinspired perovskite photodetectors with NIR-I selective photodetection and imaging capabilities by engineering precisely designed optical microcavities.[207] These biomimetic microcavities consist of alternately stacked lithium fluoride (LiF) and *N*,*N*′-bis(naphthalen-1-yl)-*N*,*N*′-bis(phenyl)benzidine (NPB) layers, with each layer's thickness precisely controlled to quarter-wavelength dimensions of the target spectrum. This NIR-I selective detection technology based on optical microcavity architecture demonstrates significant application potential in biological imaging and optical communications.

3.5.1.2 Complex structure. Usually, hierarchical light-trapping structures demonstrate superior incident light utilization efficiency compared to single photonic structures.[45] Researchers have further proposed composite structures combining multiple nanostructures to synergistically improve light extraction

efficiency while enabling polarization-selective functionalities.[43,208–210] Song *et al.* developed Moiré perovskite photodetectors with a stacked dual shallow grating structure using grating patterning (Fig. 15e).[208] The dual-grating architecture synergistically enhances light-harvesting capability and polarization sensitivity through combined diffraction effects, waveguide modes, and anti-reflection characteristics. Beyond enhancing light trapping, grating structures have demonstrated polarization-sensitive responses (Fig. 15i). Besides, Sun *et al.* integrated a moiré-grating structure into perovskite single crystals, achieving a polarization ratio of 9.1 in the fabricated photodetector.[211] Inspired by the multilevel structures of butterfly wing scales, Zhan *et al.* ingeniously constructed a 1D nano-grating bonded porous 2D PhC perovskite photodetector (Fig. 15f).[209] This design innovatively integrates multilevel optical structures with perovskite materials. This hierarchically designed composite structure ingeniously combines the diffraction properties of gratings with the photonic bandgap characteristics of PhCs, significantly enhancing the light-trapping capability of the perovskite active layer while simultaneously improving the device's photoresponse performance and enabling polarization-sensitive detection (Fig. 15j). Beyond light harvesting, biological photonic architectures have also inspired the design of advanced vision systems. In the following section, we shift our focus from energy collection to sensory perception, examining how nature's visual systems guide the development of artificial visual technologies.

3.5.2 Bioinspired visual sensing systems. Biological eyes can be primarily categorized into two types: vertebrate eyes and compound eyes.[192,193] The human eye, as a typical vertebrate eye, features all photoreceptor units sharing a single aperture and associated optical system, acquiring external visual information through unified imaging (Fig. 16a). This structure endows it with wide field-of-view, high resolution, and low aberration characteristics. In contrast, compound eyes consist of independent photoreceptive units (ommatidia), each possessing its own aperture (Fig. 16b). This architecture grants them ultra-wide field-of-view, low optical distortion, high motion sensitivity, and infinite depth-of-field properties.[212] The exquisite structures of biological eyes have inspired bionic vision system research, advancing developments in visual prosthetics, machine vision, and related fields.[213–216]

3.5.2.1 Bionic eye light-sensing vision. The development of bionic human eyes offers hope for visually impaired individuals. The core innovation in bionic human eyes lies in mimicking the structural and functional complexity of biological retinas (Fig. 16a). Typical bionic vision systems for the human eye generally comprise single-lens optical structure coupled with a curved image sensor. In 2020, Gu *et al.* successfully developed a hemispherical perovskite nanowire array retinal system (Fig. 16c and d) with the potential for high-resolution imaging comparable to the human eye.[217] They integrated high-density nanoscale photodetectors on a curved substrate. Notably, each perovskite nanowire demonstrated detectable strong photoresponse, while the porous aluminum membrane structure effectively isolated individual nanowires, significantly suppressing optical crosstalk. However, the device's resolution was limited by backside wire bonding processes. Subsequently, inspired by tunable optical structures like the crystalline lens and iris, the team further developed a bioinspired ocular device with adjustable optical components.[218] Bionic human eyes hold immense potential in the medical field, promising to restore near-natural vision for the visually impaired and enhance their quality of life. In AI and robotics, they can endow robots with more human-like vision, enabling precise object and environment recognition and advancing human–robot interaction. Insect compound eyes are intelligent imaging systems that are small-sized, multi-apertured, and wide field-of-view (Fig. 16b).[219] Insect compound eyes show high sensitivity to moving targets and strong differentiation ability regarding light intensity, wavelength, and color.[220] Hence, researching bionic insect compound eyes is highly significant (Fig. 16e). In 2024, Prof. Fan's team designed a pinhole compound eye system inspired by predatory flies (Fig. 16f and g).[221] This system features a 3D-printed hexagonal pinhole array and a hemispherical perovskite nanowire detector, achieving a 140° FOV in monocular mode and 220° in binocular configurations. It enables precise target localization and real-time tracking of quadruped robots *via* drones.

3.5.2.2 Bionic eye polarization vision. Polarization detection plays a crucial role in advanced optical sensing, offering capabilities beyond conventional intensity- or wavelength-based imaging. In remote sensing, polarization imaging can enhance detail visibility and help identify targets difficult to detect with traditional imaging. In environmental monitoring, polarization information can be used to analyze atmospheric aerosols and suspended particles in water. In information encryption and transmission, the properties of polarized light can ensure high-security data transmission. Additionally, these technologies can play significant roles in biomedical imaging and robotic vision. Many biological systems, such as mantis shrimp,[222–224] dung beetle[225] and some insect species,[226] naturally perceive polarized light, using it for navigation, communication, and prey detection. These organisms have evolved sophisticated structures—like the microvillar arrays in compound eyes—to efficiently decode polarization information from their environment.[227] For instance, desert ants (*Cataglyphis*) can forage hundreds of meters from their nest and return without getting lost. This is attributed to their polarization-sensitive compound eyes. Their photoreceptor cells have two sets of perpendicular microvilli, making them sensitive to the polarization direction of incident light (Fig. 17a–c). Inspired by desert ant eyes, Fang *et al.* used a nanoimprinting-assisted one-step solution-crystallization molding method to create a perovskite single-crystal thin film with 6400 four-directional grating arrays (Fig. 17d–f).[226]

Based on high-performance four-directional grating arrays capped perovskite single-crystal thin film, they designed a single-shot, on-chip integrated polarization photodetector without extra polarizing elements, achieving high-sensitivity

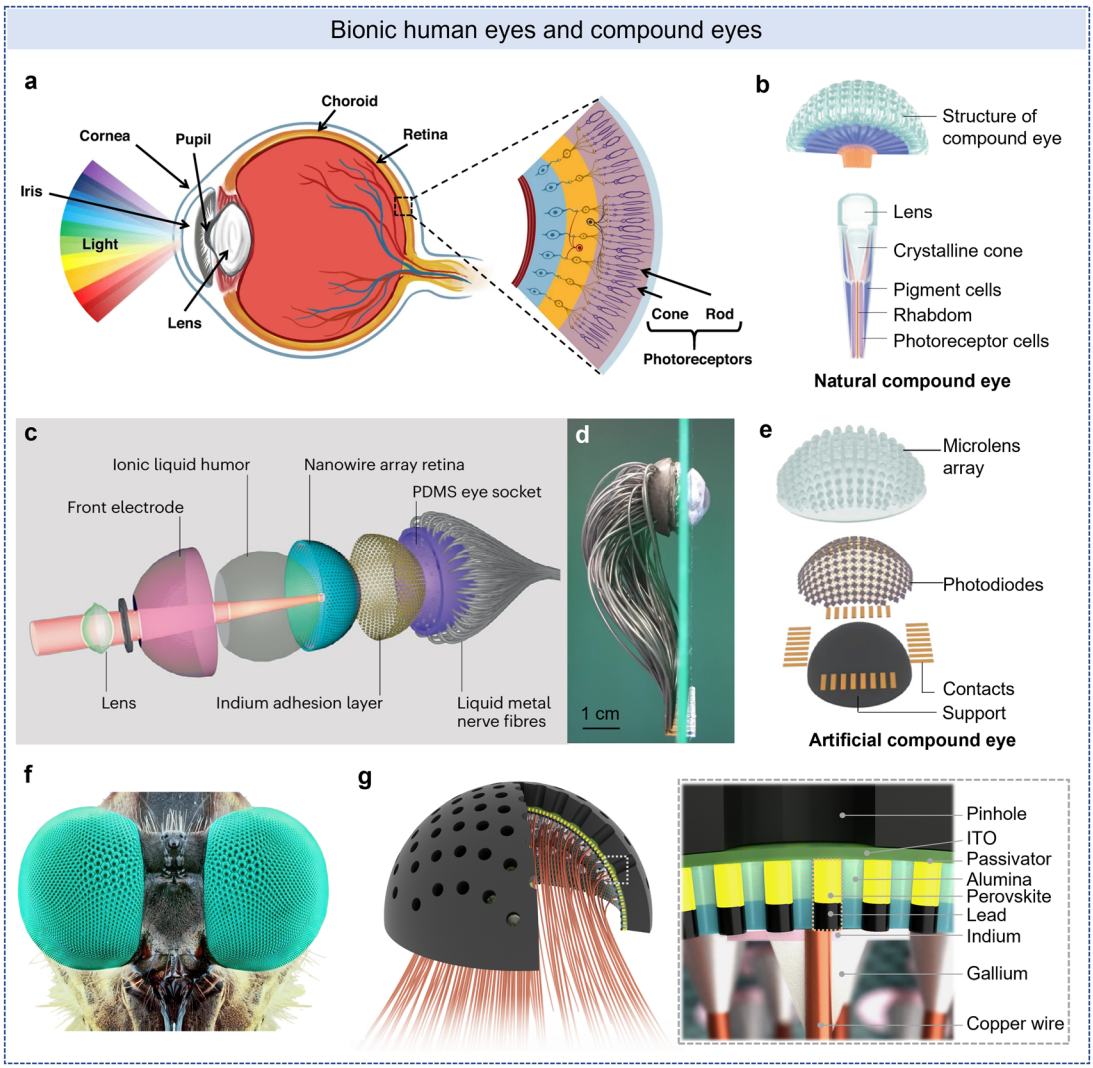

Fig. 16 Biomimetic neuronal photo-vision. (a) The human eye's anatomical structure primarily comprises the cornea, pupil, lens, vitreous body, and retina. Within the retina, photoreceptor cells (specifically cones and rods) play crucial roles in detecting light intensity and facilitating visual adaptation functions. Reproduced from ref. 213 with permission from Springer Nature, copyright 2023. (b) Structure of the compound eye (top), and structure of the ommatidium (down). Reproduced from ref. 192 with permission from Springer Nature, copyright 2024. (c) Exploded view of biomimetic electrochemical eye. (d) Side view of the biomimetic electrochemical eye. PDMS, polydimethylsiloxane. Reproduced from ref. 217 with permission from Springer Nature, copyright 2020. (e) Exploded view illustration of an artificial compound eye. Reproduced from ref. 192 with permission from Springer Nature, copyright 2024. (f) Macro photograph of a robber fly's eye. (g) Illustration exploded view of the pinhole compound eye system. Reproduced from ref. 221 with permission from AAAS, copyright 2024.

polarization imaging. This on-chip polarization detector precisely measures known angle of polarization (AoP) and degree of polarization (DoP), with accuracies of $\pm 1.2^{\circ}$ and $\pm 0.1\%$, respectively. As a proof-of-concept, the polarization photodetector has been applied in many fields including visual dehazing (Fig. 17g and h), polymer stress visualization, and detection of cancerous areas in tissues. This design offers a new approach for high-sensitivity, miniaturized, and on-chip integrated polarization imaging systems. The mantis shrimp has one of the most complex visual systems on Earth, with 16 photoreceptors to capture light of 300–720 nm wavelength and sense polarized light. Its eyes comprise numerous optical units. The middle part has six specialized ommatidia rows. Each ommatidium has different functions, including ultraviolet, linearly polarized, and circularly polarized light receptors (Fig. 17i–k). In 1999, N. J. Marshall proved mantis shrimps have linear polarization vision.[224] Their ommatidia in rows 5 and 6 have microvilli in parallel and perpendicular arrangements, forming orthogonal polarization-sensitive channels. This structure enhances polarization signal amplitude and contrast. Subsequently, researchers demonstrated that mantis shrimp can detect circularly polarized light.[222] The R8 photoreceptor, acting like a quarter-wave plate with microvilli at a precise 45°, provides the structural basis for this detection. Bionic polarization detection technologies inspired by mantis shrimp compound eyes have broad application prospects in various fields.

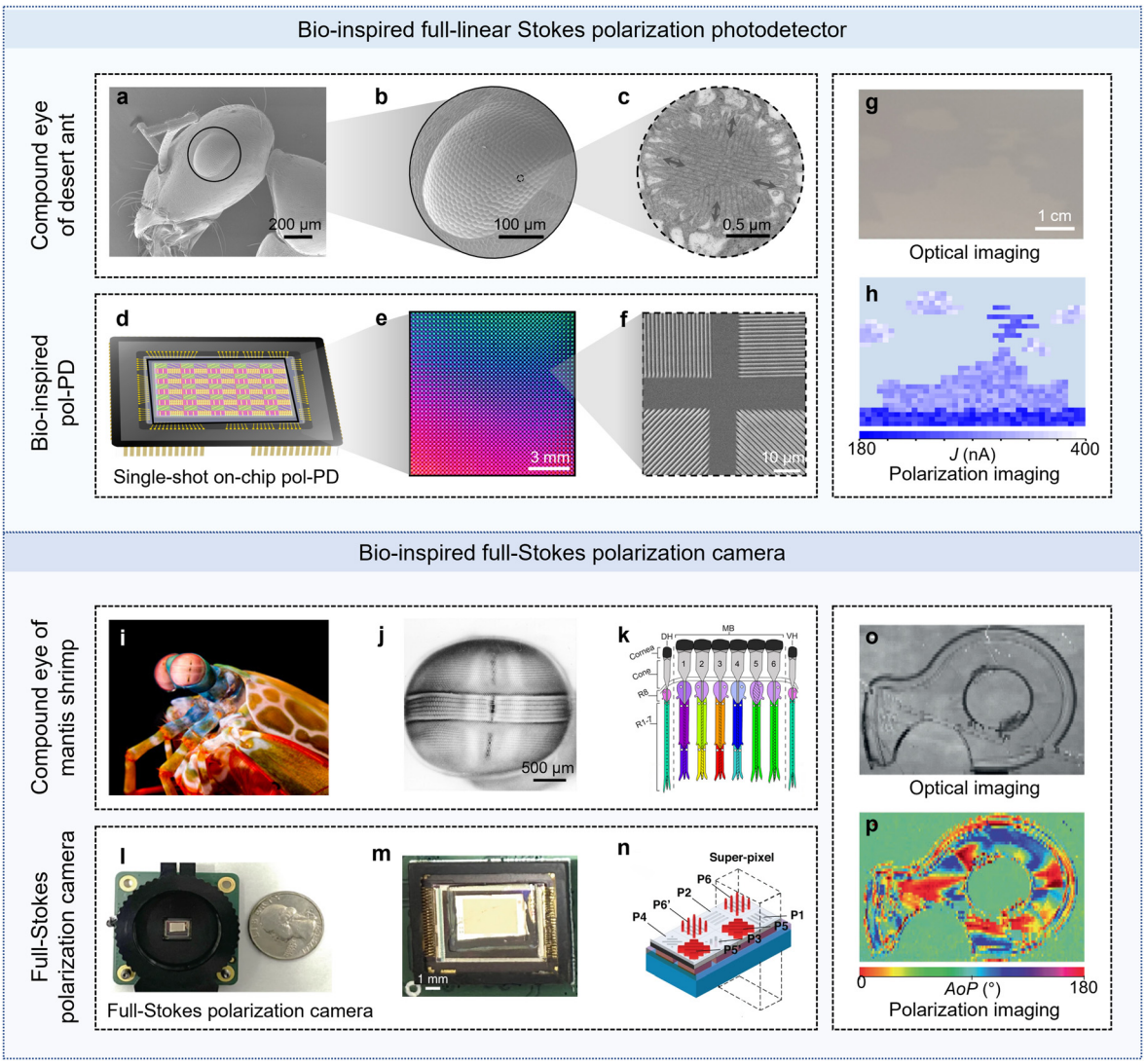

Fig. 17 Bioinspired polarization cameras. (a) SEM image of the head of *Cataglyphis*. (b) SEM image of the *Cataglyphis* compound eyes. (c) TEM image of the cross section of one small eye of the *Cataglyphis* compound eyes. There are two sets of photoreceptor microvilli perpendicular to each other. (d) Device architecture of bioinspired single-shot on-chip pol-PD. (e) Optical image of the four-directional grating arrays capped perovskite single-crystal thin film (80 by 80 pixels). (f) SEM image of a polarization unit. (g) Optical imaging of the sample. (h) Polarization imaging of sample in haze. Reproduced from ref. 226 with permission from AAAS, copyright 2024. (i) Optical image of the mantis shrimp. (j) SEM image of the compound eye of the mantis shrimp. (k) Diagrammatic sagittal section through the eye, showing the internal structure of dorsal and ventral hemispheres (DH and VH) and the six rows of the mid-band. (l) Device architecture of a full-Stokes polarization camera beside a U.S. quarter dollar coin (lens not attached). (m) Image of full Stokes polarimetric CMOS imaging sensor (n) Top: 3D Conceptual illustration of chip integrated full Stokes CMOS polarimetric imaging sensor. Here P1–P4 denotes the LP filters with transmission axes at 0°, 90°, 45°, 135° respectively. P5, P5′, and P6, P6′ denote chiral metasurface filters transmitting RCP and LCP, respectively. Here, P5 and P5′, P6 and P6′ are identical in dimensions respectively. Bottom: 2D cross-section of the chip-integrated polarimetric imaging sensor. (o) Optical imaging of the plastic ruler. (p) Polarization imaging of the plastic ruler. Reproduced from ref. 229 with permission from Springer Nature, copyright 2023.

In 2021, Michael Kudenov's team developed a mantis shrimp (stomatopod)-inspired multispectral and polarization-sensitive detector.[228] It consists of six semi-transparent polarization-sensitive organic photovoltaic detectors and polymer retarders. The design can sense 15 spectral channels over a 350-nanometer bandwidth. They also experimentally demonstrated a detector that simultaneously registered four spectral channels and three polarization channels. This system is the first to fully mimic the mantis shrimp's visual DoFs, offering a new way to enhance hyperspectral and polarization imaging by enabling simultaneous multispectral and polarization sensing along the same optical axis. Yu Yao's team at Arizona State University developed a metasurface-based full-Stokes polarization imaging sensor integrated on a chip (Fig. 17l–n).[229] They designed high performance micro-scale polarization filters, including broadband linear polarization filters and dual-color (green and red) chiral metasurfaces. Integrated into an imaging sensor, it achieved high precision polarization detection with an

average polarization measurement error of less than 2% for red and green light.

3.5.3 Light management in LEDs. LEDs have revolutionized optoelectronic technologies with their versatile applications spanning solid-state lighting, full-color displays, and biomedical sensing.[230] Modern LED architectures are primarily classified by their active-layer materials into three categories: perovskite LEDs (PeLEDs),[231] organic LEDs (OLEDs),[232] and conventional semiconductor LEDs.[194] Among these, perovskite-based LEDs have emerged as a disruptive next-generation technology, showcasing unparalleled advantages over traditional counterparts.[233,234] PeLEDs not only feature simplified fabrication processes and reduced manufacturing costs but also deliver exceptional color purity and wider gamut performance, making them ideal for ultra-high-definition displays. Notably, metal halide PeLEDs have surpassed the 20% external quantum efficiency (EQE) threshold of planar OLED configurations, with state-of-the-art devices achieving near-100% internal quantum efficiency (IQE).[195] Leveraging earth-abundant raw materials and low-energy processing techniques, PeLEDs demonstrate remarkable progress in operational stability and RGB (red, green, blue) color reproducibility, positioning them as a commercially viable solution for next-generation photonic applications.[234]

Despite remarkable advancements, state-of-the-art PeLEDs remain constrained by suboptimal EQE, primarily limited by low light OCE.[194] Approximately 80% of generated photons are trapped within the device stack through non-ideal optical coupling, leading to energy dissipation *via* lossy pathways (Fig. 18a and b).[194,195] The restricted photon extraction originates from these mechanisms: waveguide modes caused by the refractive index mismatch between perovskite layers ($\sim$2.5) and charge transport materials ($\sim$1.7–1.8); total internal reflection at substrate/air interfaces due to their refractive index contrast, confining photon emission to a narrow escape cone while trapping most photons in waveguide and substrate modes; and the evanescent SP mode at the metal/dielectric interface arises from the resonance between collective electron oscillations in the metal and electromagnetic waves. Critically, unextracted photons in these modes are converted to thermal energy, accelerating perovskite degradation and degrading device performance, ultimately suppressing EQE. Stranks *et al.* provided the EQE calculation formula for PeLEDs as follows:[235]

$$\mathrm{EQE} = f_{\mathrm{balance}} \times f_{\mathrm{e-h}} \times \eta_{\mathrm{radiative}} \times f_{\mathrm{outcoupling}}$$

where the f_{balance} is the injection balance factor of electrons and holes (when the numbers of electrons and holes injected are equal, this factor is equal to 1). The $f_{\mathrm{e-h}}$ is the likelihood of creating a correlated electron–hole pair from each pair of injected carriers. The $\eta_{\mathrm{radiative}}$ is the radiative recombination efficiency for each electron–hole pair and the $f_{\mathrm{outcoupling}}$ is the optical OCE. This formula gives us the basic guideline for PeLEDs' performance improvement. Light management strategies are therefore essential to improve the OCEs and EQEs of LEDs. Various surface or interface modification methods, such as the introduction of PhC structures, scattering structures, and optical microcavity structures have been proven to be effective in improving the OCE, based on frameworks such as waveguiding and plasmonics.[190,236]

3.5.3.1 PhC structures. The emitted light is confined within waveguide and substrate modes due to the significant disparity in the refractive index between the interfaces. PhCs can enhance the OCE of LEDs by suppressing guided-mode emission, boosting spontaneous emission *via* the Purcell effect, and facilitating light extraction across the entire surface through leaky-mode coupling.[191,237,238] Zhang *et al.* have pioneered the fabrication of PeLEDs on anodic alumina membrane (AAM) substrates, which are configured with hexagonal nanodome arrays and TiO_2 nanowire arrays (Fig. 18c and d).[239] The hexagonal nanodome arrays act as the barrier layer and the light outcoupler, and the TiO_2 nanowires function as optical antennas to enhance light extraction. The AAM has a thickness of $\sim$3 μm, a pore diameter of $\sim$120 nm, and two pitches of 500 and 1000 nm. All functional layers of the LEDs have conformal nanodome structures derived from the porous alumina membrane, with TiO_2 nanowires embedded in the pores. The higher refractive index of TiO_2 (n = 2.6) than alumina (n = 1.7) enables the TiO_2 nanowires to serve as optical antennas. Devices based on AAM with a 1000 nm pitch achieved an EQE of 17.5%, nearly double that of planar control devices (Fig. 18e). The photonic substrate in these PeLEDs facilitates a two-step light extraction process: light is coupled from the nanodome coupler to the nanowire antenna, which converts the guided modes into leaky modes for extraction as radiative light. This synergistic effect markedly improves the light extraction efficiency of PeLEDs. Shen *et al.* developed bioinspired PeLEDs by introducing a moth-eye nanostructured ZnO layer at the interface between the front electrode and the perovskite active layer using nanoimprinting.[240] The patterned ZnO served as a hole-injection layer and as an out-coupling structure to extract waveguide-mode photons. The maximum EQE of the moth-eye PeLEDs was enhanced to 20.3%, and an EQE of 28.2% was achieved with a half-ball lens. Moreover, the moth-eye PeLEDs exhibited angle-independent light emission. These findings demonstrate the nanostructure's effectiveness in extracting confined waveguide-mode photons. Furthermore, Fu *et al.* demonstrated that photonic structures integrated into functional layers can simultaneously suppress substrate modes, extract waveguide-mode light, and achieve full-area directional polarized emission through controlled light redirection.[237] Besides, using the PhCs is an effective approach to improve the OCE of OLEDs and conventional semiconductor LEDs.[238] For example, Do *et al.* demonstrated 2D SiO_2/SiN_x PhCs between ITO and glass substrate to achieve a significant OCE improvement. Wiesmann *et al.* comprehensively discussed PhC LEDs in 2009, and more theoretical details can be found in their report.[241]

3.5.3.2 Scattering structures. To extract more confined light within LEDs, it's worthwhile to adopt internal scattering structures to compensate for light losses. Modifying the active layer's

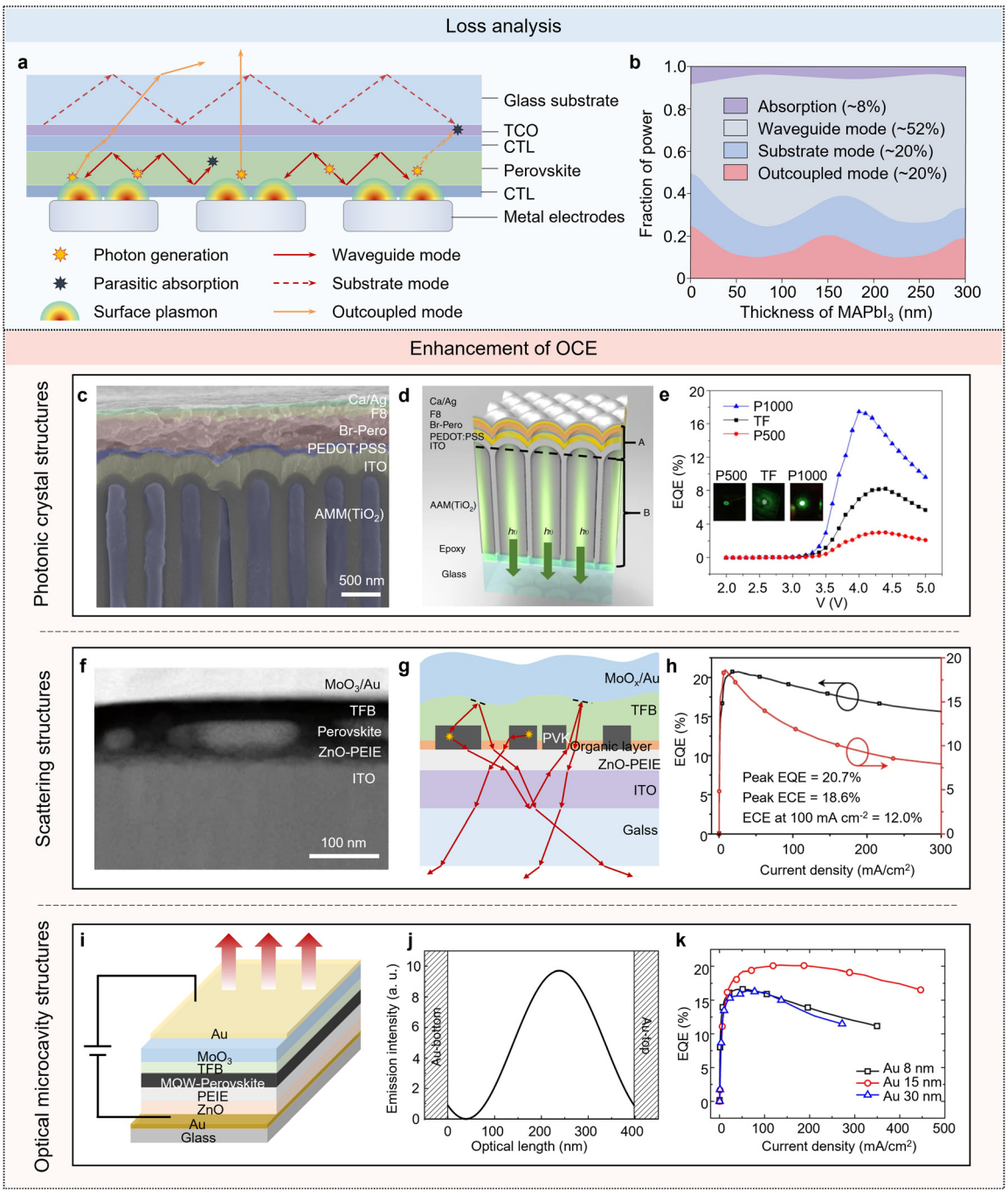

Fig. 18 Light loss analysis and enhancement of OCE in LEDs. (a) Schematic representation of the generation, propagation, emission, and losses of light in a typical planar PeLED structure. CTL, charge-transport layer. (b) Optical power distribution *versus* the thickness of emissive layer in a $MAPbI_3$ PeLED. Reproduced from ref. 195 with permission from Springer Nature, copyright 2023. (c) SEM image of an AAM-based device. Br-Pero refers to $CH_3NH_3PbBr_3$. F8 refers to poly(9,9-di-*n*-octylfluorenyl-2,7-diyl), and PEDOT:PSS refers to poly(3,4-ethylenedioxythiophene) polystyrene sulfonate. (d) Device schematic. AAM channels are filled with TiO_2. (e) EQEs of the thin film and AAM samples. Inset figures in a are the optical photos for different devices driving at 3.5 V. Reproduced from ref. 239 with permission from Springer Nature, copyright 2019. (f) Scanning tunnelling electron microscope image of a PeLED with submicrometre structures. PEIE stands for polyethylenimine ethoxylated. (g) Light trapped in devices with a continuous emitting layer, which can be extracted by the submicrometre structure. (h) EQE and ECE plotted against current density. Reproduced from ref. 244 with permission from Springer Nature, copyright 2018. (i) The device architecture of a top-emission PeLED, where a Fabry–Perot microcavity forms between two metal electrodes. The bottom Au electrode is thick and fully reflective, while the top Au film is thin and semi-transparent, allowing a small fraction of light to exit the device. (j) Emission intensity *versus* microcavity length. (k) The impact of varying the thickness of the charge injection/transport and top Au layers on the EQE. Reproduced from ref. 253 with permission from Springer Nature, copyright 2020.

morphology can enhance the light scattering in the active layer, randomize the waveguided photon paths, and boost the OCE.[233,242,243] For instance, light scattering in suitably sized crystallites offers advantages similar to those of deliberately patterned or textured structures.[242] Cao *et al.* introduced sub-micrometer-scale structures to formamidinium lead iodide-based LEDs, leading to an enhanced light outcoupling efficiency greater than 30% (Fig. 18f and g).[244] Submicron-scale structures spontaneously formed through a simple low-temperature solvent engineering approach. The resulting perovskite films (doped with 5-aminovaleric acid) exhibited a discontinuous morphology with randomly distributed planar flakes and roughly rectangular shapes, featuring grain sizes ranging from 100 to 500 nm. By leveraging structural conformality, photon structures with random concave–convex features were constructed on both the high-refractive-index perovskite layer and low-refractive-index organic functional layers. The continuous photonic cycling within these structures enables efficient extraction of light trapped in waveguide modes, thereby enhancing the OCE (Fig. 18g). This structural optimization ultimately enables the device to achieve a maximum EQE of 20.7% and a peak energy-conversion efficiency of 12% (Fig. 18h). Subsequently, Various passivation strategies have been used to reduce defect densities in discrete perovskite films, and the EQE based on the discrete perovskite films has been raised to 32.0%.[242,245–247] In OLEDs, nanoparticles patterned scattering structures have been incorporated between the substrate and the OLED structure to enhance light extraction.[248,249] These nanoparticles aid in extracting light from confined optical modes.

3.5.3.3 Optical microcavity structures. Optical microcavities can significantly enhance light outcoupling efficiency by manipulating photonic mode distribution.[250] A typical microcavity consists of a pair of parallel mirrors, including metallic reflectors (*e.g.*, Ag, semi-transparent SnO_2, or NiO), oxide-based stacks (*e.g.*, SiO_2–TiO_2), or dielectric distributed Bragg reflectors (DBRs).[251] When the emissive layer is embedded in a cavity with a thickness matching an integer multiple of the optical wavelength (*e.g.*, $\lambda/2$ or λ), the optical mode density near the emission wavelength is selectively amplified, thereby boosting spontaneous emission *via* the Purcell effect. Furthermore, phase-matching conditions from multiple-beam interference between the two mirrors enable directional control of light propagation, leading to pronounced enhancement of spontaneous emission intensity in the forward direction. Additionally, the microcavities could enhance radiative recombination rates, and reduce the electroluminescence spectral widths. By adjusting the thickness of the charge transport layers to change the cavity length, a narrowing and blue shift of the electroluminescence full width at half maximum were observed.[252] Optical microcavities offer a universal approach to boost LED performance *via* photonic confinement and interference, requiring synergistic design of resonance matching, mirror optimization, and process compatibility. Miao *et al.* showed that high-efficiency PeLEDs with a high EQE of 20.2% and an ultrahigh radiant exitance up to 114.9 mW cm^{-2} could be achieved by employing the microcavity effect to enhance light extraction (Fig. 18i–k).[253]

4. Challenges & future

In this review, we systematically overview the recent advances in bioinspired micro-nano photonic materials, mainly involving many classical natural examples, the underlying mechanisms of interaction between light and biological structures and materials, the various biomimetic materials constructed for applications in several fields. Living organisms have developed and refined materials, structures, and processes to selectively absorb, reflect, scatter, transmit, guide, and harvest light. Inspired by nature, researchers have achieved a broad range of photonic structures with relatively simple materials and under mild processing conditions.

Despite great advances and breakthroughs that have been made in recent years, three persistent challenges dominate the field: the constrained biological design exploration, the performance-directed design of multiscale ordered structures, and the scalability-reliability paradox in manufacturing. Addressing these challenges requires a paradigm shift in research methodologies, manufacturing technologies, and cross-disciplinary collaboration frameworks.

Firstly, while existing research has focused on well-characterized biological models (*e.g.*, butterfly wings, peacock feathers), over 80% of nature's photonic diversity remains unexplored. Underexplored organisms—particularly extremophiles and microorganisms—harbor unique nanostructural solutions to light management under extreme conditions. Research in bioinspired micro-nano optics encompasses not only the study of structure–property relationships in biological optical materials, but also the investigation of material formation processes (*e.g.*, biomineralization pathways, self-assembly mechanisms), which fundamentally shape the design, fabrication, characterization, and application of biomimetic materials.

Secondly, the true potential of bioinspired photonics lies in replicating nature's ability to integrate multiple optical functions within unified architectures. Biological systems achieve this through evolutionary-optimized hierarchical designs that balance competing physical requirements—a capability artificial materials currently lack. Challenges stem from incompatible material interfaces, cross-scale interference effects, and limited dynamic control mechanisms. Critical research needs span from atomic-scale material purity to macroscale system integration, bridging quantum and continuum models to achieve desired multifunctional properties (*e.g.*, energy-efficient photonics, mechanical robustness, or self-healing capability). AI-driven inverse design is emerging as a powerful strategy to address this complexity. AI-driven inverse design refers to the use of machine learning models—such as deep neural networks or generative algorithms—to automatically generate structures that meet desired optical or functional

targets. These tools invert the traditional trial-and-error process by predicting optimal architectures directly from performance requirements. While most existing models are trained on simulation datasets, biological systems adapt through continuous environmental feedback. A bioinspired AI design framework could incorporate real-time experimental inputs, such as optical performance data or environmental responses, into a closed-loop learning cycle. This approach would emulate evolutionary processes in nature and enable adaptive, context-aware design strategies beyond purely synthetic optimization.

Thirdly, the development of bioinspired photonic materials has reached a critical juncture, where breakthroughs in fundamental understanding must now translate into scalable technological solutions. Current fabrication approaches face intrinsic limitations in reconciling nanoscale precision with industrial viability. Top-down lithography techniques, while achieving atomic-scale resolution, remain energy-intensive and cost-prohibitive for large-area applications. Conversely, biomimetic self-assembly methods struggle with structural reproducibility and material compatibility. Emerging hybrid strategies combining programmable molecular assembly with advanced additive manufacturing show promise in bridging this gap. In addition, recent advances in fabrication techniques such as roll-to-roll printing, inkjet-assisted self-assembly, and template-free nanofabrication now allow high-throughput production of photonic structures over large areas while retaining optical precision. These scalable fabrication techniques have facilitated various real-world applications, including photonic textiles with durable structural colors,[254] architectural coatings,[255] anti-counterfeiting films,[256] and thermochromic printable materials for rewritable full-color displays.[257,258] Key priorities moving forward include developing self-healing materials, establishing closed-loop manufacturing cycles, and formulating standardized sustainability metrics. To support this goal, preliminary sustainability metrics have been proposed in recent studies, including fabrication energy consumption,[259] environmental toxicity of raw materials,[260] recyclability or biodegradability of structural components,[261] and operational lifetime under environmental stressors.[259] Although a unified framework remains under development, incorporating these metrics into material design and reporting standards is essential to guide the eco-responsible advancement of scalable photonic systems. Progress in these areas could substantially reduce production costs while meeting industrial performance requirements.

In summary, the ultimate goal extends beyond mimicking nature—it lies in creating adaptive photonic materials that surpass biological constraints through rational design. Potential applications span holographic encrypted information storage, intelligent optical sensors, and ultra-efficient solar energy systems. Achieving these milestones demands a highly convergent interdisciplinary collaboration across biology, optics, materials science, and artificial intelligence. By integrating biological wisdom with cutting-edge technologies, this convergence unlocks materials with unprecedented functionalities—nature's brilliance, amplified by human ingenuity. Bioinspired photonics stands as a key technology for addressing 21st-century challenges in information, energy, and environmental stewardship.

Conflicts of interest

There are no conflicts to declare.

Data availability

No primary research results, software or code have been included and no new data were generated or analysed as part of this review.

Acknowledgements

This work was financial supported by the National Science Fund for Distinguished Young Scholars (22225502), the National Natural Science Foundation of China (22435004, 22073107, and 52321006), and Bureau of International Cooperation, Chinese Academy of Sciences (027GJHZ2022044MI).

References

1 S. Hua, E. Divita, S. Yu, B. Peng, C. Roques-Carmes, Z. Su, Z. Chen, Y. Bai, J. Zou, Y. Zhu, Y. Xu, C. K. Lu, Y. Di, H. Chen, L. Jiang, L. Wang, L. Ou, C. Zhang, J. Chen, W. Zhang, H. Zhu, W. Kuang, L. Wang, H. Meng, M. Steinman and Y. Shen, *Nature*, 2025, **640**, 361–367.
2 K. Liao, Y. Lian, M. Yu, Z. Du, T. Dai, Y. Wang, H. Yan, S. Wang, C. Lu, C. T. Chan, R. Zhu, D. Di, X. Hu and Q. Gong, *Nat. Photonics*, 2025, **19**, 358–368.
3 S. Dou, H. Xu, J. Zhao, K. Zhang, N. Li, Y. Lin, L. Pan and Y. Li, *Adv. Mater.*, 2021, **33**, e2000697.
4 M. Kolle and S. Lee, *Adv. Mater.*, 2018, **30**, 1702669.
5 S. An, B. Shi, M. Jiang, B. Fu, C. Song, P. Tao, W. Shang and T. Deng, *Chem. Rev.*, 2023, **123**, 7081–7118.
6 L. P. Biró and J. P. Vigneron, *Laser Photonics Rev.*, 2010, **5**, 27–51.
7 C. Chen, Y. Kuang, S. Zhu, I. Burgert, T. Keplinger, A. Gong, T. Li, L. Berglund, S. J. Eichhorn and L. Hu, *Nat. Rev. Mater.*, 2020, **5**, 642–666.
8 D. Nepal, S. Kang, K. M. Adstedt, K. Kanhaiya, M. R. Bockstaller, L. C. Brinson, M. J. Buehler, P. V. Coveney, K. Dayal, J. A. El-Awady, L. C. Henderson, D. L. Kaplan, S. Keten, N. A. Kotov, G. C. Schatz, S. Vignolini, F. Vollrath, Y. Wang, B. I. Yakobson, V. V. Tsukruk and H. Heinz, *Nat. Mater.*, 2023, **22**, 18–35.
9 P. Vukusic, J. R. Sambles and C. R. Lawrence, *Nature*, 2000, **404**, 457.
10 S. Kinoshita, S. Yoshioka and K. Kawagoe, *Proc. R. Soc. London, Ser. B*, 2002, **269**, 1417–1421.
11 J. Zi, X. Yu, Y. Li, X. Hu, C. Xu, X. Wang, X. Liu and R. Fu, *Proc. Natl. Acad. Sci. U. S. A.*, 2003, **100**, 12576–12578.
12 M. Jacobs, M. Lopez-Garcia, O. P. Phrathep, T. Lawson, R. Oulton and H. M. Whitney, *Nat. Plants*, 2016, **2**, 16162.

13 X. Li, T. Fan, H. Zhou, S. K. Chow, W. Zhang, D. Zhang, Q. Guo and H. Ogawa, *Adv. Funct. Mater.*, 2008, **19**, 45–56.
14 K. Liu, C. Yuan, Q. Zou, Z. Xie and X. Yan, *Angew. Chem., Int. Ed.*, 2017, **56**, 7876–7880.
15 S. Enriquez, E. R. Mendez, O. Hoegh-Guldberg and R. Iglesias-Prieto, *Proc. R. Soc. London, Ser. B*, 2017, **284**, 20161667.
16 D. Wangpraseurt, S. You, F. Azam, G. Jacucci, O. Gaidarenko, M. Hildebrand, M. Kuhl, A. G. Smith, M. P. Davey, A. Smith, D. D. Deheyn, S. Chen and S. Vignolini, *Nat. Commun.*, 2020, **11**, 1748.
17 D. Wangpraseurt, S. Jacques, N. Lyndby, J. B. Holm, C. F. Pages and M. Kuhl, *J. R. Soc., Interface*, 2019, **16**, 20180567.
18 R. Xiong, J. Luan, S. Kang, C. Ye, S. Singamaneni and V. V. Tsukruk, *Chem. Soc. Rev.*, 2020, **49**, 983–1031.
19 S. Tadepalli, J. M. Slocik, M. K. Gupta, R. R. Naik and S. Singamaneni, *Chem. Rev.*, 2017, **117**, 12705–12763.
20 B. D. Wilts, B. Wijnen, H. L. Leertouwer, U. Steiner and D. G. Stavenga, *Adv. Opt. Mater.*, 2017, **5**, 1600879.
21 H. Yin, B. Dong, X. Liu, T. Zhan, L. Shi, J. Zi and E. Yablonovitch, *Proc. Natl. Acad. Sci. U. S. A.*, 2012, **109**, 10798–10801.
22 D. E. McCoy, T. Feo, T. A. Harvey and R. O. Prum, *Nat. Commun.*, 2018, **9**, 1.
23 A. Rogato and T. De Edoardo, *Growth Form*, 2023, **4**, 3–10.
24 H. Zhou, X. Li, T. Fan, F. E. Osterloh, J. Ding, E. M. Sabio, D. Zhang and Q. Guo, *Adv. Mater.*, 2010, **22**, 951–956.
25 A. Bay, P. Cloetens, H. Suhonen and J. P. Vigneron, *Opt. Express*, 2013, **21**, 764–780.
26 P. Vukusic and J. R. Sambles, *Nature*, 2003, **424**, 852–855.
27 K. Hey Tow, D. M. Chow, F. Vollrath, I. Dicaire, T. Gheysens and L. Thevenaz, *J. Lightwave Technol.*, 2018, **36**, 1138–1144.
28 Z. Hayran and F. Monticone, *Nat. Photonics*, 2025, **19**, 126–128.
29 C. Huang, Y. Luo, Y. Zhao, X. Ma, Z. Yan, Z. Liu, C. Sheng, S. Zhu and H. Liu, *Nat. Photonics*, 2024, **18**, 471–477.
30 Y. Yang, Y. Yamagami, X. Yu, P. Pitchappa, J. Webber, B. Zhang, M. Fujita, T. Nagatsuma and R. Singh, *Nat. Photonics*, 2020, **14**, 446–451.
31 Y. Li, S. Kita, P. Muñoz, O. Reshef, D. I. Vulis, M. Yin, M. Lončar and E. Mazur, *Nat. Photonics*, 2015, **9**, 738–742.
32 H. Qin, Z. Su, Z. Zhang, W. Lv, Z. Yang, W. Chen, X. Gao, H. Wei, Y. Shi, B. Li, J. Zhou, R. Fleury, C. W. Qiu and Q. Song, *Nature*, 2025, **639**, 602–608.
33 S. T. Ha, Q. Li, J. K. W. Yang, H. V. Demir, M. L. Brongersma and A. I. Kuznetsov, *Science*, 2024, **386**, eadm7442.
34 F. Chen, Y. Huang, R. Li, S. Zhang, B. Wang, W. Zhang, X. Wu, Q. Jiang, F. Wang and R. Zhang, *Chem. Commun.*, 2021, **57**, 13448–13464.
35 S. Zhou, C. Zhang, Z. Fu, Q. Zhu, Z. Zhou, J. Gong, N. Zhu, X. Wang, X. Wei, L. Xia and W. Xu, *Nat. Commun.*, 2024, **15**, 1979.
36 K. Li, T. Li, T. Zhang, H. Li, A. Li, Z. Li, X. Lai, X. Hou, Y. Wang, L. Shi, M. Li and Y. Song, *Sci. Adv.*, 2021, **7**, eabh1992.
37 Y. Liu, X. Hou, Y. Song and M. Li, *Interdiscip. Mater*, 2024, **3**, 54–73.
38 R. Li, K. Li, X. Deng, C. Jiang, A. Li, L. Xue, R. Yuan, Q. Liu, Z. Zhang, H. Li and Y. Song, *Adv. Funct. Mater.*, 2024, **34**, 2404706.
39 T. Wang, Y. Wang, Y. Fu, Z. Chen, C. Jiang, Y. E. Ji and Y. Lu, *Adv. Sci.*, 2024, **11**, e2400442.
40 X. Lai, J. Peng, Q. Cheng, A. P. Tomsia, G. Zhao, L. Liu, G. Zou, Y. Song, L. Jiang and M. Li, *Angew. Chem., Int. Ed.*, 2021, **60**, 14307–14312.
41 K. Kang, I. Byeon, Y. G. Kim, J. R. Choi and D. Kim, *Laser Photonics Rev*, 2024, **18**, 2400547.
42 S. Cui, K. Sun, Z. Liao, Q. Zhou, L. Jin, C. Jin, J. Hu, K. S. Wen, S. Liu and S. Zhou, *Sci. Bull.*, 2024, **69**, 2080–2088.
43 Y. Wang, Y. Lan, Q. Song, F. Vogelbacher, T. Xu, Y. Zhan, M. Li, W. E. I. Sha and Y. Song, *Adv. Mater.*, 2021, **33**, e2008091.
44 C. Jeffryes, J. Campbell, H. Y. Li, J. Jiao and G. Rorrer, *Energy Environ. Sci.*, 2011, **4**, 3930–3941.
45 Y. Zhan, Q. Cheng, Y. Song and M. Li, *Adv. Funct. Mater.*, 2022, **32**, 2200385.
46 Y. Fu, C. A. Tippets, E. U. Donev and R. Lopez, *Wiley Interdiscip. Rev.: Nanomed. Nanobiotechnol.*, 2016, **8**, 758–775.
47 X. Hou, F. Li, Y. Song and M. Li, *J. Phys. Chem. Lett.*, 2022, **13**, 2885–2900.
48 H. K. Raut, V. A. Ganesh, A. S. Nair and S. Ramakrishna, *Energy Environ. Sci.*, 2011, **4**, 3779.
49 X. K. Zhao, Y. Q. Xiong, W. L. Wang, W. Zhang and D. Zhang, *NPG Asia Mater.*, 2023, **15**, 20.
50 X. Ling, M. I. Osotsi, W. Zhang, Y. Wu, Q. J. Jin and D. Zhang, *J. Bionic Eng.*, 2023, **20**, 873–899.
51 W. Zhang, Y. Hu, P. Feng, Z. Li, H. Zhang, B. Zhang, D. Xu, J. Qi, H. Wang, L. Xu, Z. Li, M. Xia, J. Li, R. Chai and L. Tian, *Adv. Sci.*, 2024, **11**, e2403173.
52 G. Isapour and M. Lattuada, *Adv. Mater.*, 2018, **30**, e1707069.
53 J. Y. Sun, B. Bhushan and J. Tong, *RSC Adv.*, 2013, **3**, 14862–14889.
54 P. Tao, W. Shang, C. Song, Q. Shen, F. Zhang, Z. Luo, N. Yi, D. Zhang and T. Deng, *Adv. Mater.*, 2015, **27**, 428–463.
55 X. Cheng, Z. Shen and Y. Zhang, *Nat. Sci. Rev.*, 2024, **11**, nwad314.
56 A. Sandak and K. Butina Ogorelec, *Front. Mater.*, 2023, **10**, 1283163.
57 Q. Shen, Z. Luo, S. Ma, P. Tao, C. Song, J. Wu, W. Shang and T. Deng, *Adv. Mater.*, 2018, **30**, e1707632.
58 B. Datta, E. F. Spero, F. J. Martin-Martinez and C. Ortiz, *Adv. Mater.*, 2022, **34**, e2100939.
59 B. D. Wilts, X. Sheng, M. Holler, A. Diaz, M. Guizar-Sicairos, J. Raabe, R. Hoppe, S. H. Liu, R. Langford, O. D. Onelli, D. Chen, S. Torquato, U. Steiner, C. G. Schroer, S. Vignolini and A. Sepe, *Adv. Mater.*, 2018, **30**, e1702057.
60 S. H. Lee, S. M. Han and S. E. Han, *APL Photonics*, 2020, **5**, 056103.
61 L. Cortese, L. Pattelli, F. Utel, S. Vignolini, M. Burresi and D. S. Wiersma, *Adv. Opt. Mater.*, 2015, **3**, 1337–1341.

62 T. Lemcoff, L. Alus, J. S. Haataja, A. Wagner, G. Zhang, M. J. Pavan, V. J. Yallapragada, S. Vignolini, D. Oron, L. Schertel and B. A. Palmer, *Nat. Photonics*, 2023, **17**, 485–493.
63 R. Middleton, S. A. Tunstad, A. Knapp, S. Winters, S. McCallum and H. Whitney, *Sci. Adv.*, 2024, **10**, eadk4219.
64 B. Q. Dong, T. R. Zhan, X. H. Liu, L. P. Jiang, F. Liu, X. H. Hu and J. Zi, *Phys. Rev. E: Stat., Nonlinear, Soft Matter Phys.*, 2011, **84**, 011915.
65 G. Jacucci, S. Vignolini and L. Schertel, *Proc. Natl. Acad. Sci. U. S. A.*, 2020, **117**, 23345–23349.
66 E. R. Dufresne, H. Noh, V. Saranathan, S. G. J. Mochrie, H. Cao and R. O. Prum, *Soft Matter*, 2009, **5**, 1792–1795.
67 M. Xiao, Z. Hu, Z. Wang, Y. Li, A. D. Tormo, N. Le Thomas, B. Wang, N. C. Gianneschi, M. D. Shawkey and A. Dhinojwala, *Sci. Adv.*, 2017, **3**, e1701151.
68 Z. Wang, R. Li, Y. Zhang, C. L. C. Chan, J. S. Haataja, K. Yu, R. M. Parker and S. Vignolini, *Adv. Mater.*, 2023, **35**, 2207923.
69 V. Hwang, A. B. Stephenson, S. Barkley, S. Brandt, M. Xiao, J. Aizenberg and V. N. Manoharan, *Proc. Natl. Acad. Sci. U. S. A.*, 2021, **118**, e2015551118.
70 G. Zhang and M. Xiao, *Opt. Express*, 2024, **32**, 20432.
71 V. E. Johansen, O. D. Onelli, L. M. Steiner and S. Vignolini, *Functional Surfaces in Biology III*, Springer International Publishing, 2017, ch. 3, pp. 53–89, DOI: **10.1007/978-3-319-74144-4_3**.
72 P. D. Kaplan, A. D. Dinsmore, A. G. Yodh and D. J. Pine, *Phys. Rev. E: Stat. Phys., Plasmas, Fluids, Relat. Interdiscip. Top.*, 1994, **50**, 4827–4835.
73 L. F. Rojas-Ochoa, J. M. Mendez-Alcaraz, J. J. Sáenz, P. Schurtenberger and F. Scheffold, *Phys. Rev. Lett.*, 2004, **93**, 073903.
74 J. Lee, T. Terlier, Y. J. Jang, K. B. Lee and Y. Lee, *Surf. Interface Anal.*, 2020, **52**, 656–664.
75 S. Berthier, *Optical Biomimetics*, Woodhead, Woodhead, 2012, pp. 79–115e, DOI: **10.1533/9780857097651.79**.
76 B. Frka-Petesic, T. G. Parton, C. Honorato-Rios, A. Narkevicius, K. Ballu, Q. Shen, Z. Lu, Y. Ogawa, J. S. Haataja, B. E. Droguet, R. M. Parker and S. Vignolini, *Chem. Rev.*, 2023, **123**, 12595–12756.
77 S. Vignolini, P. J. Rudall, A. V. Rowland, A. Reed, E. Moyroud, R. B. Faden, J. J. Baumberg, B. J. Glover and U. Steiner, *Proc. Natl. Acad. Sci. U. S. A.*, 2012, **109**, 15712–15715.
78 L. T. McDonald, E. D. Finlayson, B. D. Wilts and P. Vukusic, *Interface Focus*, 2017, **7**, 20160129.
79 V. Sharma, M. Crne, J. O. Park and M. Srinivasarao, *Science*, 2009, **325**, 449–451.
80 K. Zhang, S. J. Zhou, Y. W. Tang, G. Wang, H. Zhou, T. X. Fan and D. Zhang, *RSC Adv.*, 2014, **4**, 51865–51871.
81 M. Kolle, P. M. Salgard-Cunha, M. R. Scherer, F. Huang, P. Vukusic, S. Mahajan, J. J. Baumberg and U. Steiner, *Nat. Nanotechnol.*, 2010, **5**, 511–515.
82 H. Zhou, J. Xu, X. Liu, H. Zhang, D. Wang, Z. Chen, D. Zhang and T. Fan, *Adv. Funct. Mater.*, 2017, **28**, 1705309.
83 D. E. McCoy, V. E. McCoy, N. K. Mandsberg, A. V. Shneidman, J. Aizenberg, R. O. Prum and D. Haig, *Proc. R. Soc. London, Ser. B*, 2019, **286**, 20190589.
84 Q. Zhao, X. Guo, T. Fan, J. Ding, D. Zhang and Q. Guo, *Soft Matter*, 2011, **7**, 11433.
85 A. L. Davis, H. F. Nijhout and S. Johnsen, *Nat. Commun.*, 2020, **11**, 1294.
86 A. S. Fiorucci and C. Fankhauser, *Curr. Biol.*, 2017, **27**, R931–R940.
87 Z. Tong, D. Yang, Z. Li, Y. Nan, F. Ding, Y. Shen and Z. Jiang, *ACS Nano*, 2017, **11**, 1103–1112.
88 J. H. Sun, J. S. Zhang, M. W. Zhang, M. Antonietti, X. Z. Fu and X. C. Wang, *Nat. Commun.*, 2012, **3**, 1139.
89 J. Liu, Q. Yang, W. T. Yang, M. Z. Li and Y. L. Song, *J. Mater. Chem. A*, 2013, **1**, 7760–7766.
90 X. W. Sun, Y. X. Zhang and D. Losic, *J. Mater. Chem. A*, 2017, **5**, 8847–8859.
91 J. W. Goessling, W. P. Wardley and M. Lopez-Garcia, *Adv. Sci.*, 2020, **7**, 1903726.
92 E. De Tommasi, *J. Spectrosc.*, 2016, **2016**, 1–13.
93 R. Hünig, A. Mertens, M. Stephan, A. Schulz, B. Richter, M. Hetterich, M. Powalla, U. Lemmer, A. Colsmann and G. Gomard, *Adv. Opt. Mater.*, 2016, **4**, 1487–1493.
94 J. J. Kim, Y. Lee, H. G. Kim, K. J. Choi, H. S. Kweon, S. Park and K. H. Jeong, *Proc. Natl. Acad. Sci. U. S. A.*, 2012, **109**, 18674–18678.
95 P. Mao, C. Liu, X. Li, M. Liu, Q. Chen, M. Han, S. A. Maier, E. H. Sargent and S. Zhang, *Light: Sci. Appl.*, 2021, **10**, 180.
96 A. Yoshida, M. Motoyama, A. Kosaku and K. Miyamoto, *Zool. Sci.*, 1997, **14**, 737–741.
97 N. Huby, V. Vié, A. Renault, S. Beaufils, T. Lefèvre, F. Paquet-Mercier, M. Pézolet and B. Bêche, *Appl. Phys. Lett.*, 2013, **102**, 123702.
98 J. Li, S. Li, J. Huang, A. Q. Khan, B. An, X. Zhou, Z. Liu and M. Zhu, *Adv. Sci.*, 2022, **9**, e2103965.
99 D. E. McCoy, D. H. Burns, E. Klopfer, L. K. Herndon, B. Ogunlade, J. A. Dionne and S. Johnsen, *Nat. Commun.*, 2024, **15**, 9445.
100 M. M. Ito, A. H. Gibbons, D. Qin, D. Yamamoto, H. Jiang, D. Yamaguchi, K. Tanaka and E. Sivaniah, *Nature*, 2019, **570**, 363–367.
101 S. U. Kim, Y. J. Lee, J. Liu, D. S. Kim, H. Wang and S. Yang, *Nat. Mater.*, 2022, **21**, 41–46.
102 A. Kristensen, J. K. W. Yang, S. I. Bozhevolnyi, S. Link, P. Nordlander, N. J. Halas and N. A. Mortensen, *Nat. Rev. Mater.*, 2016, **2**, 16088.
103 X. Hou, F. Li, Y. Song and M. Li, *J. Phys. Chem. Lett.*, 2022, **13**, 2885–2900.
104 J. B. Kim, C. Chae, S. H. Han, S. Y. Lee and S. H. Kim, *Sci. Adv.*, 2021, **7**, eabj8780.
105 D. Y. Kim, M. J. Kim, G. Sung and J. Y. Sun, *Nano Converge.*, 2019, **6**, 21.
106 Y. Zhao, Y. Zhao, S. Hu, J. Lv, Y. Ying, G. Gervinskas and G. Si, *Materials*, 2017, **10**, 944.
107 Y. Sun, Y. Wang, Y. Liu, S. Wu, S. Zhang and W. Niu, *Adv. Funct. Mater.*, 2022, **32**, 2204467.

108 Q. Shi, J. Liang, X. Wang, K. Yao, Y. Tang, C. Pan, J. Sun, R. Liu, H. Tan and T. Tang, *Chem. Eng. J.*, 2024, **485**, 149966.
109 G. H. Lee, T. M. Choi, B. Kim, S. H. Han, J. M. Lee and S.-H. Kim, *ACS Nano*, 2017, **11**, 11350–11357.
110 G. Bogdanov, A. A. Strzelecka, N. Kaimal, S. L. Senft, S. Lee, R. T. Hanlon and A. A. Gorodetsky, *Science*, 2025, **388**, 1389–1395.
111 Y. Wang, Q. Zhao and X. Du, *Mater. Horiz.*, 2020, **7**, 1341–1347.
112 Q. Fu, W. Yu, G. Bao and J. Ge, *Nat. Commun.*, 2022, **13**, 7007.
113 W. Li, Y. Wang, M. Li, L. P. Garbarini and F. G. Omenetto, *Adv. Mater.*, 2019, **31**, 1901036.
114 Y. Z. Yang, X. Zhang, C. Valenzuela, R. Bi, Y. H. Chen, Y. Liu, C. Zhang, W. B. Li, L. Wang and W. Feng, *Matter*, 2024, **7**, 1–17.
115 A. E. Goodling, S. Nagelberg, B. Kaehr, C. H. Meredith, S. I. Cheon, A. P. Saunders, M. Kolle and L. D. Zarzar, *Nature*, 2019, **566**, 523–527.
116 K. Li, T. Li, T. Zhang, H. Li, A. Li, Z. Li, X. Lai, X. Hou, Y. Wang, L. Shi, M. Li and Y. Song, *Sci. Adv.*, 2021, **7**, eabh1992.
117 P. Cencillo-Abad, D. Franklin, P. Mastranzo-Ortega, J. Sanchez-Mondragon and D. Chanda, *Sci. Adv.*, 2023, **9**, eadf7207.
118 D. Franklin, Z. He, P. Mastranzo Ortega, A. Safaei, P. Cencillo-Abad, S. T. Wu and D. Chanda, *Proc. Natl. Acad. Sci. U. S. A.*, 2020, **117**, 13350–13358.
119 S. Sun, W. Yang, C. Zhang, J. Jing, Y. Gao, X. Yu, Q. Song and S. Xiao, *ACS Nano*, 2018, **12**, 2151–2159.
120 X. Liu, Z. Huang and J. Zang, *Nano Lett.*, 2020, **20**, 8739–8744.
121 W. Yang, S. Xiao, Q. Song, Y. Liu, Y. Wu, S. Wang, J. Yu, J. Han and D.-P. Tsai, *Nat. Commun.*, 2020, **11**, 1864.
122 R. R. Sahu, A. S. Ramasamy, S. Bhonsle, M. Vailshery, A. S, H. Kumar and T. Das Gupta, *Nat. Nanotechnol.*, 2024, **19**, 766–774.
123 J. Geng, L. Xu, W. Yan, L. Shi and M. Qiu, *Nat. Commun.*, 2023, **14**, 565.
124 F. Neubrech, X. Duan and N. Liu, *Sci. Adv.*, 2020, **6**, eabc2709.
125 Z. Li and Y. Yin, *Adv. Mater.*, 2019, **31**, e1807061.
126 C. Li, X. Zhou, K. Wang, K. Li, M. Li and Y. Song, *Chem. Commun.*, 2019, **12**, 47–53.
127 K. Chen, Q. Fu, S. Ye and J. Ge, *Adv. Funct. Mater.*, 2017, **27**, 1702825.
128 W. Yu, Y. Zhao, W. Sheng and J. Ge, *Adv. Funct. Mater.*, 2023, **33**, 2304474.
129 Q. Fu, Y. Zhao, W. Yu and J. Ge, *Chem. Eng. J.*, 2025, **505**, 159050.
130 W. Yu, Y. Zhao and J. Ge, *J. Colloid Interface Sci.*, 2024, **659**, 603–610.
131 B. H. Miller, H. Liu and M. Kolle, *Nat. Mater.*, 2022, **21**, 1014.
132 X. Hou, F. Vogelbacher, X. Lai, K. Li, Y. Song and M. Li, *Sci. Bull.*, 2023, **68**, 276–283.
133 D. Franklin, Y. Chen, A. Vazquez-Guardado, S. Modak, J. Boroumand, D. Xu, S. T. Wu and D. Chanda, *Nat. Commun.*, 2015, **6**, 7337.
134 H. Zheng, W. Li, W. Li, X. Wang, Z. Tang, S. X. Zhang and Y. Xu, *Adv. Mater.*, 2018, **30**, e1705948.
135 Y. J. Hongkyu Eoh, C. Park, C. Eun Lee, T. Hyun Park, H. Sol Kang, S. Jeon, D. Yeol Ryu, J. Huh and C. Park, *Adv. Funct. Mater.*, 2021, **32**, 2103697.
136 Q. Zhou, J. G. Park, J. Bae, D. Ha, J. Park, K. Song and T. Kim, *Adv. Mater.*, 2020, **32**, e2001467.
137 G. Qu, W. Yang, Q. Song, Y. Liu, C. W. Qiu, J. Han, D. P. Tsai and S. Xiao, *Nat. Commun.*, 2020, **11**, 5484.
138 D. Wen, F. Yue, G. Li, G. Zheng, K. Chan, S. Chen, M. Chen, K. F. Li, P. W. H. Wong, K. W. Cheah, E. Yue Bun Pun, S. Zhang and X. Chen, *Nat. Commun.*, 2015, **6**, 8241.
139 M. Khorasaninejad, A. Ambrosio, P. Kanhaiya and F. Capasso, *Sci. Adv.*, 2016, **2**, e1501258.
140 P. Chen, C. Wang, D. Wei, Y. Hu, X. Xu, J. Li, D. Wu, J. Ma, S. Ji, L. Zhang, L. Xu, T. Wang, C. Xu, J. Chu, S. Zhu, M. Xiao and Y. Zhang, *Light: Sci. Appl.*, 2021, **10**, 146.
141 R. Zhao, B. Sain, Q. Wei, C. Tang, X. Li, T. Weiss, L. Huang, Y. Wang and T. Zentgraf, *Light: Sci. Appl.*, 2018, **7**, 95.
142 I. Kim, J. Jang, G. Kim, J. Lee, T. Badloe, J. Mun and J. Rho, *Nat. Commun.*, 2021, **12**, 3614.
143 H. Ren, X. Fang, J. Jang, J. Burger, J. Rho and S. A. Maier, *Nat. Nanotechnol.*, 2020, **15**, 948–955.
144 X. Ouyang, Y. Xu, M. Xian, Z. Feng, L. Zhu, Y. Cao, S. Lan, B.-O. Guan, C.-W. Qiu, M. Gu and X. Li, *Nat. Photonics*, 2021, **15**, 901–907.
145 I. Kim, W. S. Kim, K. Kim, M. A. Ansari, M. Q. Mehmood, T. Badloe, Y. Kim, J. Gwak, H. Lee, Y. K. Kim and J. Rho, *Sci. Adv.*, 2021, **7**, eabe9943.
146 P. Zheng, Q. Dai, Z. Li, Z. Ye, J. Xiong, H. C. Liu, G. Zheng and S. Zhang, *Sci. Adv.*, 2021, **7**, eabg0363.
147 Z. L. Deng, Q. A. Tu, Y. Wang, Z. Q. Wang, T. Shi, Z. Feng, X. C. Qiao, G. P. Wang, S. Xiao and X. Li, *Adv. Mater.*, 2021, **33**, e2103472.
148 F. Dong and W. Chu, *Adv. Mater.*, 2019, **31**, e1804921.
149 Z. Zhao, Z. Wang, Y. Shi, S. Wan and Z. Li, *Adv. Mater.*, 2025, **37**, 2419322.
150 X. Lai, Q. Ren, F. Vogelbacher, W. E. I. Sha, X. Hou, X. Yao, Y. Song and M. Li, *Adv. Mater.*, 2022, **34**, 2107243.
151 X. Lai, T. Li, X. Hou, F. Vogelbacher, J. Wang, Y. Song, L. Shi and M. Li, *Proc. Natl. Acad. Sci. U. S. A.*, 2025, **122**, e2419113122.
152 W. Wang, Y. Zhou, L. Yang, X. Yang, Y. Yao, Y. Meng and B. Tang, *Adv. Funct. Mater.*, 2022, **32**, 2204744.
153 W. Hong, Z. Yuan and X. Chen, *Small*, 2020, **16**, e1907626.
154 T. Lee, J. Jang, H. Jeong and J. Rho, *Nano Converge.*, 2018, **5**, 1.
155 J. Xue, Y. Wang, T. Zhang, K. Li, F. Vogelbacher, Y. Zhang, X. Hou, Z. Zhu, Y. Tian, Y. Song and M. Li, *Sci. China: Chem.*, 2023, **66**, 3567–3575.
156 Q. Ruan, W. Zhang, H. Wang, J. Y. E. Chan, H. Wang, H. Liu, D. Fan, Y. Li, C. W. Qiu and J. K. W. Yang, *Adv. Mater.*, 2021, **34**, 2108128.

157 H. Huang, H. Li, J. Yin, K. Gu, J. Guo and C. Wang, *Adv. Mater.*, 2023, **35**, 2211117.
158 M. Lu, X. Zhang, D. Xu, N. Li and Y. Zhao, *Adv. Mater.*, 2023, **35**, e2211330.
159 K. Yao, Q. Meng, V. Bulone and Q. Zhou, *Adv. Mater.*, 2017, **29**, 1701323.
160 A. Ng, R. Telles, K. S. Riley, J. A. Lewis, C. C. Cook, E. Lee and S. Yang, *Adv. Mater.*, 2025, **37**, e2416621.
161 Z. Zhang, C. Wang, Q. Wang, Y. Zhao and L. Shang, *Proc. Natl. Acad. Sci. U. S. A.*, 2022, **119**, e2204113119.
162 X. Yang, Z. Zhang, H. Sun, Y. Yun, H. Xie, Z. Tan, H. Wang, Y. Yang, B. Chen, H. Teng, X. Pan, M. Yang, Y. Sun, Y. Song and M. Su, *J. Am. Chem. Soc.*, 2025, **147**, 3383–3391.
163 S. H. Nah, J. B. Kim, H. N. T. Chui, Y. Suh and S. Yang, *Adv. Mater.*, 2024, **36**, e2409297.
164 S. Dou, H. Xu, J. Zhao, K. Zhang, N. Li, Y. Lin, L. Pan and Y. Li, *Adv. Mater.*, 2020, **33**, 2000697.
165 J. Liu, H. Tang, C. Jiang, S. Wu, L. Ye, D. Zhao and Z. Zhou, *Adv. Funct. Mater.*, 2022, **32**, 2206962.
166 M. Lee, G. Kim, Y. Jung, K. R. Pyun, J. Lee, B. W. Kim and S. H. Ko, *Light: Sci. Appl.*, 2023, **12**, 134.
167 X. Ling, M. I. Osotsi, W. Zhang, Y. Wu, Q. Jin and D. Zhang, *J. Bionic Eng.*, 2022, **20**, 873–899.
168 H. Zhang, Q. He, F. Zhang, Y. Duan, M. Qin and W. Feng, *Adv. Mater.*, 2025, **37**, 202503140.
169 S. Fan and W. Li, *Nat. Photonics*, 2022, **16**, 182–190.
170 X. Yin, R. Yang, G. Tan and S. Fan, *Science*, 2020, **370**, 786–791.
171 N. N. Shi, C.-C. Tsai, F. Camino, G. D. Bernard, N. Yu and R. Wehner, *Science*, 2015, **349**, 298–301.
172 D. Zhao and H. Tang, *Science*, 2023, **382**, 644–645.
173 K. Lin, S. Chen, Y. Zeng, T. C. Ho, Y. Zhu, X. Wang, F. Liu, B. Huang, C. Y.-H. Chao, Z. Wang and C. Y. Tso, *Science*, 2023, **382**, 691–697.
174 Y. Chen, J. Mandal, W. Li, A. Smith-Washington, C. C. Tsai, W. Huang, S. Shrestha, N. Yu, R. P. S. Han, A. Cao and Y. Yang, *Sci. Adv.*, 2020, **6**, eaaz5413.
175 L. Cai, Y. Peng, J. Xu, C. Zhou, C. Zhou, P. Wu, D. Lin, S. Fan and Y. Cui, *Joule*, 2019, **3**, 1478–1486.
176 X. Wang, Q. Zhang, S. Wang, C. Jin, B. Zhu, Y. Su, X. Dong, J. Liang, Z. Lu, L. Zhou, W. Li, S. Zhu and J. Zhu, *Sci. Bull.*, 2022, **67**, 1874–1881.
177 S. Son, S. Jeon, D. Chae, S. Y. Lee, Y. Liu, H. Lim, S. J. Oh and H. Lee, *Nano Energy*, 2021, **79**, 105461.
178 Y. Yin, P. Sun, Y. Zeng, M. Yang, S. Gao, S. Wang, Z. Huang, Y. Zhang, Y. Wang and Z. Wang, *Adv. Energy Mater.*, 2024, **14**, 2402202.
179 Y. Lin, C. Qin, Z. Liang, W. Lin, J. Wang and D. Li, *Adv. Opt. Mater.*, 2024, **12**, 2401020.
180 C. Sheng, Y. An, J. Du and X. Li, *ACS Photonics*, 2019, **6**, 2545–2552.
181 G. P. Wang, W. Zhang, L. Sun, B. Hong, X. Yan, X. Zhao, X. Shu, H. Xing and W. Wang, *Optica*, 2023, **10**, 1059–1066.
182 G. J. Lee, Y. J. Kim, H. M. Kim, Y. J. Yoo and Y. M. Song, *Adv. Opt. Mater.*, 2018, **6**, 1800707.
183 W. Li, Y. Shi, Z. Chen and S. Fan, *Nat. Commun.*, 2018, **9**, 4240.
184 W. Zhu, B. Droguet, Q. Shen, Y. Zhang, T. G. Parton, X. Shan, R. M. Parker, M. F. L. De Volder, T. Deng, S. Vignolini and T. Li, *Adv. Sci.*, 2022, **9**, 2202061.
185 X. Hou, K. Zhang, X. Lai, L. Hu, F. Vogelbacher, Y. Song, L. Jiang and M. Li, *Matter*, 2025, **8**, 101898.
186 H. Huang, H. Li, X. Shen, K. Gu, J. Guo and C. Wang, *Chem. Eng. J.*, 2022, **429**, 132437.
187 C. Li, A. Ke, H. Shen and X. Zhang, *J. Mater. Chem. A*, 2025, **13**, 18833–18841.
188 M. L. Brongersma, Y. Cui and S. Fan, *Nat. Mater.*, 2014, **13**, 451–460.
189 I. Massiot, A. Cattoni and S. Collin, *Nat. Energy*, 2020, **5**, 959–972.
190 S.-F. Leung, Q. Zhang, F. Xiu, D. Yu, J. C. Ho, D. Li and Z. Fan, *J. Phys. Chem. Lett.*, 2014, **5**, 1479–1495.
191 Y. Zhan, C. Li, Z. Che, H. C. Shum, X. Hu and H. Li, *Energy Environ. Sci.*, 2023, **16**, 4135–4163.
192 Z. Long, Y. Zhou, Y. Ding, X. Qiu, S. Poddar and Z. Fan, *Nat. Rev. Mater.*, 2024, **10**, 128–146.
193 Z. Long, Y. Ding, S. Poddar, L. Gu, Q. Zhang and Z. Fan, *Mater. Today Electron.*, 2023, **6**, 100071.
194 Q. Zhang, D. Zhang, Y. Fu, S. Poddar, L. Shu, X. Mo and Z. Fan, *Adv. Funct. Mater.*, 2020, **30**, 2002570.
195 B. Zhao, M. Vasilopoulou, A. Fakharuddin, F. Gao, A. R. B. Mohd Yusoff, R. H. Friend and D. Di, *Nat. Nanotechnol.*, 2023, **18**, 981–992.
196 J. Zhang, J. Zhao, Y. Zhou, Y. Wang, K. S. Blankenagel, X. Wang, M. Tabassum and L. Su, *Adv. Opt. Mater.*, 2021, **9**, 2100524.
197 Y. Wang, P. Wang, X. Zhou, C. Li, H. Li, X. Hu, F. Li, X. Liu, M. Li and Y. Song, *Adv. Energy Mater.*, 2018, **8**, 1702960.
198 K. Deng, Z. Liu, M. Wang and L. Li, *Adv. Funct. Mater.*, 2019, **29**, 1900830.
199 H. Lee and H. J. Kim, *Electron. Mater. Lett.*, 2022, **18**, 407–414.
200 G. Hu, J. Guo, J. Jiang, L. Wang, J. Zhang, H. Chen, G. Lou, W. Wei and L. Shen, *Light: Sci. Appl.*, 2025, **14**, 61.
201 Y. Zhu, L. Shu, S. Poddar, Q. Zhang, Z. Chen, Y. Ding, Z. Long, S. Ma, B. Ren, X. Qiu and Z. Fan, *Nano Lett.*, 2022, **22**, 9586–9595.
202 J. Peng, D. Walter, Y. Ren, M. Tebyetekerwa, Y. Wu, T. Duong, Q. Lin, J. Li, T. Lu, M. A. Mahmud, O. L. C. Lem, S. Zhao, W. Liu, Y. Liu, H. Shen, L. Li, F. Kremer, H. T. Nguyen, D. Y. Choi, K. J. Weber, K. R. Catchpole and T. P. White, *Science*, 2021, **371**, 390–395.
203 Y. Wang, M. Li, X. Zhou, P. Li, X. Hu and Y. Song, *Nano Energy*, 2018, **51**, 556–562.
204 M. M. Tavakoli, K.-H. Tsui, Q. Zhang, J. He, Y. Yao, D. Li and Z. Fan, *ACS Nano*, 2015, **9**, 10287–10295.
205 J. Wei, R. P. Xu, Y. Q. Li, C. Li, J. D. Chen, X. D. Zhao, Z. Z. Xie, C. S. Lee, W. J. Zhang and J. X. Tang, *Adv. Energy Mater.*, 2017, **7**, 1700492.
206 S. M. Kang, S. Jang, J. K. Lee, J. Yoon, D. E. Yoo, J. W. Lee, M. Choi and N. G. Park, *Small*, 2016, **12**, 2443–2449.
207 F. Cao, J. Chen, D. Yu, S. Wang, X. Xu, J. Liu, Z. Han, B. Huang, Y. Gu, K. L. Choy and H. Zeng, *Adv. Mater.*, 2020, **32**, e1905362.

208 Q. Song, Y. Wang, F. Vogelbacher, Y. Zhan, D. Zhu, Y. Lan, W. Fang, Z. Zhang, L. Jiang, Y. Song and M. Li, *Adv. Energy Mater.*, 2021, **11**, 2100742.
209 Y. Zhan, Y. Wang, Q. Cheng, C. Li, K. Li, H. Li, J. Peng, B. Lu, Y. Wang, Y. Song, L. Jiang and M. Li, *Angew. Chem., Int. Ed.*, 2019, **58**, 16456–16462.
210 Y. Zhan, Q. Cheng, J. Peng, Y. Zhao, F. Vogelbacher, X. Lai, F. Wang, Y. Song and M. Li, *Nano Energy*, 2022, **98**, 107254.
211 S. X. Li, H. Xia, T. Y. Liu, H. Zhu, J. C. Feng, Y. An, X. L. Zhang and H. B. Sun, *Adv. Mater.*, 2023, **35**, 2207771.
212 K.-H. Jeong, J. Kim and L. P. Lee, *Science*, 2006, **312**, 557–561.
213 W. Liu, X. Yang, Z. Wang, Y. Li, J. Li, Q. Feng, X. Xie, W. Xin, H. Xu and Y. Liu, *Light: Sci. Appl.*, 2023, **12**, 180.
214 X. Luo, C. Chen, Z. He, M. Wang, K. Pan, X. Dong, Z. Li, B. Liu, Z. Zhang, Y. Wu, C. Ban, R. Chen, D. Zhang, K. Wang, Q. Wang, J. Li, G. Lu, J. Liu, Z. Liu and W. Huang, *Nat. Commun.*, 2024, **15**, 3086.
215 Y. Liu, Z. Ji, G. Cen, H. Sun, H. Wang, C. Zhao, Z. L. Wang and W. Mai, *Light: Sci. Appl.*, 2023, **12**, 43.
216 Z. Rao, Y. Lu, Z. Li, K. Sim, Z. Ma, J. Xiao and C. Yu, *Nat. Electron.*, 2021, **4**, 513–521.
217 L. Gu, S. Poddar, Y. Lin, Z. Long, D. Zhang, Q. Zhang, L. Shu, X. Qiu, M. Kam, A. Javey and Z. Fan, *Nature*, 2020, **581**, 278–282.
218 Z. Long, X. Qiu, C. L. J. Chan, Z. Sun, Z. Yuan, S. Poddar, Y. Zhang, Y. Ding, L. Gu, Y. Zhou, W. Tang, A. K. Srivastava, C. Yu, X. Zou, G. Shen and Z. Fan, *Nat. Commun.*, 2023, **14**, 1972.
219 Y. M. Song, Y. Xie, V. Malyarchuk, J. Xiao, I. Jung, K. J. Choi, Z. Liu, H. Park, C. Lu, R. H. Kim, R. Li, K. B. Crozier, Y. Huang and J. A. Rogers, *Nature*, 2013, **497**, 95–99.
220 Y. Long, B. Dai, C. Chang, N. Upreti, L. Wei, L. Zheng, S. Zhuang, T. J. Huang and D. Zhang, *Sci. Adv.*, 2025, **11**, eadt3505.
221 Y. Zhou, Z. Sun, Y. Ding, Z. Yuan, X. Qiu, Y. B. Cao, Z. A. Wan, Z. Long, S. Poddar, S. Kumar, W. Ye, C. L. J. Chan, D. Zhang, B. Ren, Q. Zhang, H.-S. Kwok, M. G. Li and Z. Fan, *Sci. Robot.*, 2024, **9**, eadi8666.
222 I. M. Daly, M. J. How, J. C. Partridge, S. E. Temple, N. J. Marshall, T. W. Cronin and N. W. Roberts, *Nat. Commun.*, 2016, **7**, 12140.
223 J. Marshall, T. W. Cronin and S. Kleinlogel, *Arthropod Struct. Dev.*, 2007, **36**, 420–448.
224 H. H. Thoen, M. J. How, T.-H. Chiou and J. Marshall, *Science*, 2014, **343**, 411–413.
225 J. Pan, S. Chen, S. Chen, J. Wang, M. Su, R. Jia, J. Jie and X. Zhang, *Adv. Mater.*, 2025, **37**, e2415530.
226 W. Fang, C. Liu, Z. Zhu, C. Wu, Q. Cheng, Q. Song, Y. Wang, X. Lai, Y. Song, L. Jiang and M. Li, *Sci. Adv.*, 2024, **10**, eadr5375.
227 G. Horváth, *Polarized Light and Polarization Vision in Animal Sciences*, Springer Berlin, Heidelberg, 2014.
228 A. Altaqui, P. Sen, H. Schrickx, J. Rech, J.-W. Lee, M. Escuti, W. You, B. J. Kim, R. Kolbas, B. T. O'Connor and M. Kudenov, *Sci. Adv.*, 2021, **7**, eabe3196.
229 J. Zuo, J. Bai, S. Choi, A. Basiri, X. Chen, C. Wang and Y. Yao, *Light: Sci. Appl.*, 2023, **12**, 218.
230 B. R. Sutherland and E. H. Sargent, *Nat. Photonics*, 2016, **10**, 295–302.
231 T.-H. Han, K. Y. Jang, Y. Dong, R. H. Friend, E. H. Sargent and T.-W. Lee, *Nat. Rev. Mater.*, 2022, **7**, 757–777.
232 Y. R. Do, Y.-C. Kim, Y.-W. Song and Y.-H. Lee, *J. Appl. Phys.*, 2004, **96**, 7629–7636.
233 K. Lin, J. Xing, L. N. Quan, F. P. G. de Arquer, X. Gong, J. Lu, L. Xie, W. Zhao, D. Zhang, C. Yan, W. Li, X. Liu, Y. Lu, J. Kirman, E. H. Sargent, Q. Xiong and Z. Wei, *Nature*, 2018, **562**, 245–248.
234 M. Zhang, X. Ma, J. L. Esguerra, H. Yu, O. Hjelm, J. Li and F. Gao, *Nat. Sustain.*, 2025, **8**, 315–324.
235 S. D. Stranks, R. L. Z. Hoye, D. Di, R. H. Friend and F. Deschler, *Adv. Mater.*, 2019, **31**, e1803336.
236 C. Cho, B. Zhao, G. D. Tainter, J.-Y. Lee, R. H. Friend, D. Di, F. Deschler and N. C. Greenham, *Nat. Commun.*, 2020, **11**, 611.
237 X. Fu, Y. Mehta, Y. A. Chen, L. Lei, L. Zhu, N. Barange, Q. Dong, S. Yin, J. Mendes, S. He, R. Gogusetti, C. H. Chang and F. So, *Adv. Mater.*, 2021, **33**, e2006801.
238 B. J. Matterson, J. M. Lupton, A. F. Safonov, M. G. Salt, W. L. Barnes and I. D. W. Samuel, *Adv. Mater.*, 2001, **13**, 123–127.
239 Q. Zhang, M. M. Tavakoli, L. Gu, D. Zhang, L. Tang, Y. Gao, J. Guo, Y. Lin, S. F. Leung, S. Poddar, Y. Fu and Z. Fan, *Nat. Commun.*, 2019, **10**, 727.
240 Y. Shen, L. P. Cheng, Y. Q. Li, W. Li, J. D. Chen, S. T. Lee and J. X. Tang, *Adv. Mater.*, 2019, **31**, e1901517.
241 C. Wiesmann, K. Bergenek, N. Linder and U. T. Schwarz, *Laser Photonics Rev.*, 2009, **3**, 262–286.
242 M. Li, Y. Yang, Z. Kuang, C. Hao, S. Wang, F. Lu, Z. Liu, J. Liu, L. Zeng, Y. Cai, Y. Mao, J. Guo, H. Tian, G. Xing, Y. Cao, C. Ma, N. Wang, Q. Peng, L. Zhu, W. Huang and J. Wang, *Nature*, 2024, **630**, 631–635.
243 W. Xu, Q. Hu, S. Bai, C. Bao, Y. Miao, Z. Yuan, T. Borzda, A. J. Barker, E. Tyukalova, Z. Hu, M. Kawecki, H. Wang, Z. Yan, X. Liu, X. Shi, K. Uvdal, M. Fahlman, W. Zhang, M. Duchamp, J.-M. Liu, A. Petrozza, J. Wang, L.-M. Liu, W. Huang and F. Gao, *Nat. Photonics*, 2019, **13**, 418–424.
244 Y. Cao, N. Wang, H. Tian, J. Guo, Y. Wei, H. Chen, Y. Miao, W. Zou, K. Pan, Y. He, H. Cao, Y. Ke, M. Xu, Y. Wang, M. Yang, K. Du, Z. Fu, D. Kong, D. Dai, Y. Jin, G. Li, H. Li, Q. Peng, J. Wang and W. Huang, *Nature*, 2018, **562**, 249–253.
245 Z. Liu, W. Qiu, X. Peng, G. Sun, X. Liu, D. Liu, Z. Li, F. He, C. Shen, Q. Gu, F. Ma, H. L. Yip, L. Hou, Z. Qi and S. J. Su, *Adv. Mater.*, 2021, **33**, e2103268.
246 Y. Chen, R. Wang, G. Kusch, B. Xu, C. Hao, C. Xue, L. Cheng, L. Zhu, J. Wang, H. Li, R. A. Oliver, N. Wang, W. Huang and J. Wang, *Nat. Commun.*, 2025, **16**, 3254.
247 Y. Sun, L. Ge, L. Dai, C. Cho, J. Ferrer Orri, K. Ji, S. J. Zelewski, Y. Liu, A. J. Mirabelli, Y. Zhang, J. Y. Huang, Y. Wang, K. Gong, M. C. Lai, L. Zhang, D. Yang, J. Lin, E. M. Tennyson, C. Ducati, S. D. Stranks, L. S. Cui and N. C. Greenham, *Nature*, 2023, **615**, 830–835.

248 S. A. Choulis, M. K. Mathai and V.-E. Choong, *Appl. Phys. Lett.*, 2006, **88**, 213503.
249 J. Y. Kim, C. S. Choi, W. H. Kim, D. Y. Kim, D. H. Kim and K. C. Choi, *Opt. Express*, 2013, **21**, 5424–5431.
250 E. F. Schubert, N. E. J. Hunt, M. Micovic, R. J. Malik, D. L. Sivco, A. Y. Cho and G. J. Zydzik, *Science*, 1994, **265**, 943–945.
251 T.-Y. Cho, C.-L. Lin and C.-C. Wu, *Appl. Phys. Lett.*, 2006, **88**, 111106.
252 S. Hofmann, M. Thomschke, B. Lüssem and K. Leo, *Opt. Express*, 2011, **19**, A1250–A1264.
253 Y. Miao, L. Cheng, W. Zou, L. Gu, J. Zhang, Q. Guo, Q. Peng, M. Xu, Y. He, S. Zhang, Y. Cao, R. Li, N. Wang, W. Huang and J. Wang, *Light: Sci. Appl.*, 2020, **9**, 89.
254 Y. He, L. Liu, Q. Fu and J. Ge, *Adv. Funct. Mater.*, 2022, **32**, 2200330.
255 C. Wang, X. Lin, C. G. Schäfer, S. Hirsemann and J. Ge, *Adv. Funct. Mater.*, 2021, **31**, 2008601.
256 J. Wang, F. Pang, Q. Fu and J. Ge, *Sci. China Mater.*, 2022, **66**, 1623–1631.
257 X. Zhang, Y. Ran, Q. Fu and J. Ge, *Small*, 2022, **18**, 2106533.
258 X. Zhang, T. Yin and J. Ge, *Adv. Mater.*, 2023, **36**, 2309344.
259 R. Vaz, M. F. Frasco and M. G. F. Sales, *Nanoscale Adv.*, 2020, **2**, 5106–5129.
260 Y.-X. Zhang, Y. Wang, K. Zhang, D. Liu, R. Fatima, Y. Li and D.-P. Song, *Adv. Mater.*, 2025, **37**, 2501303.
261 X. Ma, B. Wu, L. Hou and P. Wu, *ACS Nano*, 2025, **19**, 23945–23954.

